Dark matter haloes: an additional criterion for the choice of fitting density profiles

R. Caimmi and C. Marmo*

February 2, 2008

Abstract

Simulated dark matter haloes are fitted by self-similar, universal density profiles, where the scaled parameters depend only on a scaled (truncation) radius, $\Xi = R/r_0$, which, in turn, is supposed to be independent on the mass and the formation redshift. The further assumption of a lognormal distribution (for a selected mass bin) of the scaled radius, or concentration, in agreement with the data from a large statistical sample of simulated haloes (Bullock et al. 2001), allows (at least to a first extent) a normal or lognormal distribution for other scaled parameters, via the same procedure which leads to the propagation of the errors. A criterion for the choice of the best fitting density profile is proposed, with regard to a set of high-resolution simulations, where some averaging procedure on scaled density profiles has been performed, in connection with a number of fitting density profiles. To this aim, a minimum value of the ratio, $|x_{\overline{\eta}}|/\sigma_{s\,\overline{\eta}} = |\overline{\eta} - \eta^*|/\sigma_{s\,\overline{\eta}}$, is required to yield the best fit, where $\overline{\eta}$ is the arithmetic mean over the whole set; η^* is its counterpart related to the fitting density profile; $\sigma_{s\,\overline{\eta}}$ is the standard deviation from the mean; and η is a selected,

*Astronomy Department, Padua Univ., Vicolo Osservatorio 2, I-35122 Padova, Italy
email: caimmi@pd.astro.it

scaled i.e. dimensionless parameter. The above criterion is applied to a pair of sets each made of a dozen of high-resolution simulations, FM01 (Fukushige & Makino 2001) and KLA01 (Klypin et al. 2001), in connection with two currently used fitting density profiles, NFW (e.g., Navarro et al. 1997) and MOA (e.g., Moore et al. 1999), where the dependence of the scaled radius on the mass and the formation redshift, may be neglected to a first extent. With regard to FM01 and KLA01 samples, the best fits turn out to be MOA and NFW, respectively. In addition, the above results also hold in dealing with rms errors derived via the propagation of the errors, with regard to the distributions of scaled parameters. The sensitivity error of simulations is also estimated and shown to be less than the related, standard deviation, that is a necessary condition for detectability of accidental errors. Some features of the early evolution of dark matter haloes represented by fitting density profiles, are discussed in the limit of the spherical top-hat model. Though the related matter distributions appear to be poorly representative of simulated haloes, unless the (mean) peak height is an increasing function of the mass, the results are shown to be consistent, provided considerable acquisition of angular momentum takes place during the expansion phase.
keywords - cosmology: dark matter.

1 Introduction

According to a wide number of both analytical and numerical studies (e.g., Cole & Lacey 1996; Syer & White 1998; Navarro et al. 1995, 1996, 1997, hereafter quoted as NFW97; Moore et al. 1998, 1999, hereafter quoted as MOA99; Fukushige & Makino 2001, hereafter quoted as FM01; Klypin et al. 2001, hereafter quoted as KLA01; Fukushige & Makino 2003, hereafter quoted as FM03), dark matter haloes which virialize from hierarchical clustering show universal density profiles, $\rho = \rho(r; \rho_0, r_0)$, where ρ_0 is a scaling density and r_0 is a scaling radius. In this view, smaller haloes formed first from initial density fluctuations and then merged with each other, or were tidally disrupted from previously formed mergers, to become larger haloes.

The density profile is (i) self-similar, in the sense that it has the same expression, independent of time (e.g., FM01), and (ii) universal, in the sense that it has the same expression, independent of halo mass, initial density

perturbation spectrum, or value of cosmological parameters (e.g., NFW97; FM01; FM03). A satisfactory fit to the results of numerical simulations is the family of density profiles (e.g., Hernquist 1990; Zhao 1996):

$$\rho\left(\frac{r}{r_0}\right) = \frac{\rho_0}{(r/r_0)^\gamma[1+(r/r_0)^\alpha]^\chi} \quad ; \quad \chi = \frac{\beta-\gamma}{\alpha} \quad ; \tag{1}$$

for a suitable choice of exponents, α, β, and γ.

This family includes both cuspy profiles first proposed by Navarro et al. (1995, 1996), NFW97, $(\alpha,\beta,\gamma) = (1,3,1)$, hereafter quoted as NFW density profile, and the so called modified isothermal profile, $(\alpha,\beta,\gamma) = (2,2,0)$, which is the most widely used model for the halo density distribution in analyses of observed rotation curves. It also includes the perfect ellipsoid (e.g., De Zeeuw 1985), $(\alpha,\beta,\gamma) = (2,4,0)$, which is the sole (known) ellipsoidal density profile where a test particle admits three global integrals of motion. Finally, it includes the Hernquist (1990) density profile, $(\alpha,\beta,\gamma) = (1,4,1)$, which closely approximates the de Vaucouleurs $r^{1/4}$ law for elliptical galaxies. In dealing with the formation of dark matter haloes from hierarchical clustering in both CDM and ΛCDM scenarios, recent high-resolution simulations allow $(\alpha,\beta,\gamma) = (3/2,3,3/2)$, hereafter quoted as MOA density profile, as a best fit (e.g., Ghigna et al. 2000; FM01; KLA01; FM03), as first advocated by Moore et al. (1998) and MOA99[1]. But for a different point of view, concerning the trend near the centre of the system, see e.g. Mücket & Hoeft (2003).

In addition, purely dark matter structures which fulfill Jeans equation, exhibit $-3 \leq \gamma \leq -1$ for density profiles following an exact power-law, $\rho \propto r^{-\gamma}$, and this constraint weakens only slightly for a more general mass distribution where the density-power slope, $\gamma(r)$, is a function of the radius; if otherwise, the system cannot be considered as in equilibrium and/or the effects of baryionic component have to be investigated (Hansen 2004).

Leaving aside peculiar situations such as the occurrence of major mergers, the average evolution may be approximated as self-similar to a good extent. Accordingly, a single halo may be characterized by two parameters: the (fiducial) total mass, M, and a dimensionless quantity, δ, related to the amplitude of the density perturbation at the collapse (NFW97, FM01). The

[1]More precisely, a slope $\alpha = 1.4$ was derived by Moore et al. (1998), while the value $\alpha = 1.5$ was established in MOA99.

scaling density, ρ_0, and the scaling radius, r_0, may also be expressed in terms of M and δ (NFW97, FM01).

Though Eq. (1) implies null density at infinite radius, profile fits are necessarily performed within the virialized region of a halo, bounded by a truncation radius. The presence of neighbouring systems makes the tidal radius as an upper limit. On the other hand, isolated objects cannot extend outside the Hubble sphere of equal mass. The region enclosed within the truncation boundary has to be intended as representative of the quasi static halo interior, leaving aside the surrounding material which is still infalling. Numerical simulations show that the quasi static halo interior is defined by a mean density, $\bar{\rho}_{200} \approx 200\rho_{crit}$ (e.g., Cole & Lacey 1996; NFW97; FM01), where ρ_{crit} is the critical density of the universe. An alternative definition is found in KLA01, where the quasi static halo interior has same mean density as predicted by the top-hat model.

Given a set of simulated, dark matter haloes, the choice of a fitting density profile, expressed by Eq. (1), implies the following steps (e.g., Dubinski & Carlberg 1991; FM01; KLA01; FM03).

(a) Select a choice of exponents (α, β, γ), for defining the universal density profile.

(b) Use a nonlinear least-squares method to determine the best fit for the scaling density, ρ_0, and the scaling radius, r_0, with regard to each simulation.

(c) Determine the scaled, averaged density profile, and related values of the scaling parameters, $(\overline{r}_0, \overline{\rho}_0)$.

(d) Particularize the fitting formula, expressed by Eq. (1), to $(r_0, \rho_0) = (\overline{r}_0, \overline{\rho}_0)$, and calculate the parameters of interest, including the residuals related to the scaled, averaged and fitting density profile.

At present, no general consensus exists on the details of the above mentioned procedure. The scaling density and the scaling radius may be constrained to yield $M(R) = M_{trn}$, where $M(R)$ is the mass within the truncation radius, R, related to the fitting density profile, and M_{trn} is the mass within the virialized region (e.g., FM03). An average all over the simulations may be performed with regard to the scaling density and the scaling radius, or

any other two equivalent parameters (e.g., FM01). The minimization procedure may be applied on the sum of either the squares of logarithmic residuals, $[\log(\rho_{sim}/\rho_0) - \log(\rho_{uni}/\rho_0)]^2$ (e.g., Dubinski & Carlberg 1991; FM03), or the absolute values of logarithmic residuals, $|\log(\rho_{sim}/\rho_0) - \log(\rho_{uni}/\rho_0)|$ (e.g., KLA01), where ρ_{sim} and ρ_{uni} denote simulated and universal density profile, respectively, related to an assigned radius, r. For further details on the fitting procedures see e.g., Fukushige et al. (2004), Tasitsiomi et al. (2004).

Though the above mentioned method allows a selection between different, universal density profiles (e.g., FM01, FM03), it does not seem to hold in general (e.g., KLA01). In other words a simulated density profile may be fitted, to an acceptable extent, by universal density profiles with several choices of exponents, (α, β, γ), appearing in Eq. (1). Further investigation on additional criterions, in fitting universal to simulated density profiles, could be useful in lowering the above mentioned degeneracy.

Data from a statistical sample of about five thousands of simulated, dark matter haloes (Bullock et al. 2001), are consistent with a lognormal distribution of the concentration, $\Xi_{trn} = R/r_0$, i.e. the ratio of the truncation radius, R, to the scaling radius, r_0, with regard to NFW density profiles. The distribution is related to masses within a range (0.5-1.0)$\times 10^n h^{-1}\mathrm{M}_\odot$, where $11 \leq n \leq 14$ and n is an integer. The scatter is large, of about $\sigma_{\log \Xi_{trn}} = 0.18$ (Bullock et al. 2001).

The existence of a lognormal distribution is a necessary, but not sufficient condition, for the validity of the central limit theorem. In this view, the concentration is related to the final properties of a simulated halo, which are connected with the initial conditions, α_1, α_2, ..., α_n, by a transformation, $\Xi_{trn} = \alpha_1 \alpha_2 ... \alpha_n$, as in dealing with the process of star formation, where the stellar mass follows a lognormal distribution (for further details, see Adams & Fatuzzo 1996; Padoan et al. 1997).

If, for a selected mass range, the density profile is assumed to be universal, then the scaled physical parameters, related to e.g., mass, moment of inertia, and potential energy, depend on the scaled radius only (e.g., Caimmi & Marmo 2003). Accordingly, the distribution of a scaled physical parameter, to a first extent, is expected to be normal or lognormal.

There is a well known analogon of the above procedure in the theory of errors. Let a physical quantity, Ξ, be directly measured, and then follow a normal distribution, characterized by an expected value, Ξ^*, and a rms error, σ_Ξ. Let one other physical quantity, Ψ, depend on the former one,

$\Psi = \phi(\Xi)$, and then be indirectly measured. As a result of the theory of errors, the physical quantity, Ψ, at least to a first extent, also follows a normal distribution, characterized by an expected value, $\Psi^* = \phi(\Xi^*)$, and a rms error, $\sigma_\Psi = |(\partial\phi/\partial\Xi)_{\Xi^*}|\sigma_\Xi$.

The current investigation is aimed to provide an additional criterion in fitting universal to simulated density profiles. The related procedure starts from a set of high-resolution simulations, where (i) both mass and radius of the virialized region are known for each sample halo; (2) scaled density profiles are averaged over the whole sample; (3) scaling parameters, (r_0, ρ_0), are deduced with regard to different choices of exponents, (α, β, γ), which appear in the fitting formula, expressed by Eq. (1).

A fitting, scaled density profile, is defined by a choice of exponents, (α, β, γ), and a scaled truncation radius, Ξ, which allows the calculation of the remaining scaled parameters. Under the assumption of invariant, scaled truncation radius, a fitting, scaled density profile represents a family of infinite density profiles, hereafter quoted as *fitting scaled halo*, each related to a particular choice of scaling parameters, (r_0, ρ_0). Accordingly, the generic member of the above mentioned family is defined by three exponents, (α, β, γ), a scaled truncation radius, Ξ, and two scaling parameters, (r_0, ρ_0).

A similar situation occurs for polytropes (e.g., Caimmi 1980), where a scaled density profile represents a family of infinite density profiles. It depends on one exponent, n (the polytropic index), and a scaled radius, Ξ (where the density falls to zero). The generic member of the family depends, in addition, on two scaling parameters, (R, λ), which represent the radius and the central density, respectively.

Given a sample of simulated, dark matter haloes, let us define a mean, scaled density profile, as the result of some averaging procedure over the whole sample. Then a mean, scaled density profile represents its parent set of simulations and, in the following, it shall be quoted as *mean scaled halo*.

With regard to a selected, fitting, scaled density profile, (α, β, γ), the dependence of the scaling parameters, (r_0, ρ_0), on a pair of independent parameters, (M, δ), can be deduced from the mean, scaled halo (e.g., FM01). Then a scaled mass, M/M_0, can be explicitly expressed and compared with its counterpart related to the fitting, scaled density profile. It, in turn, allows the calculation of the scaled truncation radius, Ξ, and other scaled parameters, which define the fitting scaled halo.

On the other hand, in dealing with a generic, simulated halo, both mass and radius of the virialized region, M_{trn} and R_{trn}, are known as computer outputs. Accordingly, a scaled radius, $\xi_{trn} = r_{trn}/r_0$, and a scaled mass, M_{trn}/M_0, can be determined together with additional scaled parameters, and the deviations from their counterparts, related to the fitting, scaled halo, may be analysed. In particular, the arithmetic mean, $\overline{\eta}$, the standard deviation from the mean, $\sigma_{s\,\overline{\eta}}$, and the standard deviation from the standard deviation from the mean, $\sigma_{s\,\overline{\mu}}$, may be calculated for a selected scaled parameter, η.

The fitting density profile to a fixed simulated halo, is defined by three exponents, (α, β, γ), a scaled truncation radius, ξ_{trn}, and two scaling parameters, (r_0, ρ_0). It shall be hereafter quoted as *fitting halo*. Unlike the fitting, scaled halo, fitting haloes exhibit different scaled truncation radii, related to different simulated haloes, while the remaining parameters are left unchanged.

At this stage, it is possible to see to what extent different, fitting, scaled density profiles, (α, β, γ), make scaled parameters, η, related to each simulated halo, deviate from their counterparts, η^*, related to the fitting, scaled halo. In other words, one is able to recognize if the inequality, $\overline{\eta} - \sigma_{s\,\overline{\eta}} < \eta^* < \overline{\eta} + \sigma_{s\,\overline{\eta}}$, is fulfilled. Finally, the best fitting density profile among the ones under consideration, is chosen as minimizing the ratio, $|x_{\overline{\eta}}|/\sigma_{s\,\overline{\eta}} = |\overline{\eta} - \eta^*|/\sigma_{s\,\overline{\eta}}$.

The current investigation shall be limited to samples of recent, high-resolution, virialized structures where (a) the sample is homogeneous i.e. related to a fixed cosmological model; (b) the sample is not extremely poor i.e. the number of objects exceeds ten; (c) the values of the scaling density, scaling radius, virial mass, and virial radius, are reported or may be deduced from the results.

The above conditions are satisfied by two samples, each made of a dozen of runs, namely FM01 and KLA01. With regard to the latter, the twelve runs studied therein are in fact three sets of simulations of only four dark matter haloes with resolution varied in each set. They cannot be treated as twelve independent runs but, on the other hand, they can be conceived as measures of a same physical quantity, but using different methods.

The two sets of runs differ in many respects, namely: 1) cosmological model; 2) criterium in making subsets of runs; 3) criterium in ending simulations; 4) mass range; 5) definition of the virial radius; 6) scaling between NFW and MOA density profiles; 7) choice of the pair of independent parameters, i.e. (M, δ) or (ρ_0, r_0). For further details, see FM01 and KLA01.

Both NFW and MOA density profiles are fitted to simulated density profiles for the samples under consideration (FM01, KLA01). Accordingly, the above mentioned criterion shall be used in the present paper, to see what is the best fit, among NFW and MOA, to each set of simulations.

The main limit of the current approach lies in the assumption of scaled density profiles, related to an invariant, scaled (truncation) radius, Ξ, and other scaled parameters depending only on Ξ. In general, the scaled radius, which has the same formal definition as the concentration (e.g., NFW97), depends on both the mass and the redshift. More precisely, the concentration is lowered for increasing mass (constant redshift) and redshift (constant mass), with a milder/steeper dependence for CDM/ΛCDM cosmological models (Bullok et al. 2001). An investigation based on a large statistical sample (Bullok et al. 2001) has shown that, within a ΛCDM scenario, the intrinsic spread in concentration related to a mass bin of distinct haloes, is comparable to the systematic change in the mean value of concentration related to the above mentioned mass bin, across the entire mass range studied therein ($10^{11} < M/\mathrm{M}_{\odot} < 10^{14}$).

It will be shown that, for both FM01 and KLA01 simulations, the intrinsic spread in concentration is dominant over the systematic change in the mean value of concentration on a mass bin, across the entire mass range studied therein. Accordingly, the fitting density profile may be considered, to an acceptable extent, as related to an invariant scaled radius. In general, it is the case for a sufficiently narrow mass range.

The current paper is organized in the following way. Useful formulae related to NFW and MOA density profiles are summarized in section 2. The fitting, scaled haloes, related to FM01 and KLA01 set of simulations, with regard to both NFW and MOA density profiles, are determined in section 3. The deviations of simulated haloes from their fitting counterparts, in connection with a number of scaled parameters, is also analysed therein. The following section 4 is dedicated to a discussion, within which some features of the early evolution of fitting haloes are discussed, in the limit of the spherical top-hat model. Some concluding remarks are drawn in section 5. Further investigation on a few special arguments is performed in the Appendix.

2 NFW and MOA density profiles

With regard to the family of density profiles, expressed by Eq. (1), let us define a scaled density, f, and a scaled radius, ξ, as:

$$f(\xi) = \frac{\rho}{\rho_0} = \frac{2^\chi}{\xi^\gamma (1+\xi^\alpha)^\chi} \quad ; \qquad f(1) = 1 \quad ; \tag{2}$$

$$\xi = \frac{r}{r_0} \quad ; \qquad \Xi = \frac{R}{r_0} \quad ; \tag{3}$$

where the normalization, $f(1) = 1$, makes ρ_0 and r_0 be the density and the radius (i.e. radial coordinate), respectively, of a reference isopycnic surface, and Ξ corresponds to the truncation isopycnic surface, or the truncation radius, R. On the other hand, the normalization currently used in the literature takes $\rho_0' = 2^\chi \rho_0$, in particular $(\rho_0')_{NFW} = 4\rho_0$ and $(\rho_0')_{MOA} = 2\rho_0$. The choice of exponents, $(\alpha, \beta, \gamma) = (1, 3, 1)$, $(3/2, 3, 3/2)$, selects NFW and MOA density profiles, respectively, from Eq. (1).

The explicit expression of a number of scaled parameters, related to global or local properties of the parent density profile, are listed in Tab. 1. Local properties depend on the scaled radius, ξ, and global properties depend on the scaled truncation radius, Ξ, which has the same formal definition as the concentration (e.g., NFW97).

3 Mean and fitting dark matter haloes

It can be shown that both NFW and MOA density profiles provide an acceptable fit to high-resolution simulations (e.g., FM01; KLA01), with the possible exception of scales of the order of cluster of galaxies, where MOA density profiles seem to be preferred with respect to NFW density profiles (e.g., FM03).

The explicit expression of the scaling density, ρ_0, as a function of the independent parameters, (M, δ), prescribed in FM01, by averaging over the whole set of simulations, reads:

$$\rho_0 = C_\rho \delta \left(\frac{M}{\mathrm{M}_{10}}\right)^{-1} \frac{\mathrm{M}_{10}}{\mathrm{kpc}^3} \quad ; \quad \mathrm{M}_{10} = 10^{10}\mathrm{M}_\odot \quad ; \tag{4a}$$

$$(C_\rho)_{NFW,FM} = \frac{7k_1^3}{40} \quad ; \quad (C_\rho)_{MOA,FM} = \frac{7}{20} \quad ; \tag{4b}$$

function or parameter	definition	NFW	MOA
$f(\xi)$	$\frac{\rho(\xi)}{\rho_0}$	$\frac{4}{\xi(1+\xi)^2}$	$\frac{2}{\xi^{3/2}(1+\xi^{3/2})}$
$P(\xi)$	$2\int f(\xi)\xi\,\mathrm{d}\xi$	$\frac{8}{1+\xi}$	$-2[\omega_1(\xi)+\omega_2(\xi)+\omega_3(\xi)]$
$F(\xi)$	$2\int_\xi^\Xi f(\xi)\xi\,\mathrm{d}\xi$	$P(\Xi)-P(\xi)$	$P(\Xi)-P(\xi)$
ν_M	$\frac{M}{M_0}$	$12\left[\ln(1+\Xi)-\frac{\Xi}{1+\Xi}\right]$	$4\ln(1+\Xi^{3/2})$
$\nu_{\bar\rho}$	$\frac{\bar\rho}{\rho_0}$	$\frac{12}{\Xi^3}\left[\ln(1+\Xi)-\frac{\Xi}{1+\Xi}\right]$	$\frac{4}{\Xi^3}\ln(1+\Xi^{3/2})$
ν_{eq}	$\frac{v_{eq}(\Xi)}{(v_0)_{eq}}$	$\left[\frac{1}{\Xi}\frac{\ln(1+\Xi)-\Xi/(1+\Xi)}{\ln 2-1/2}\right]^{1/2}$	$\left[\frac{1}{\Xi}\frac{\ln(1+\Xi^{3/2})}{\ln 2}\right]^{1/2}$
ν_I	$\frac{I}{2MR^2}$	$\frac{6(1+\Xi)\ln(1+\Xi)+\Xi^3-3\Xi^2-6\Xi}{9\Xi^2[(1+\Xi)\ln(1+\Xi)-\Xi]}$	$\frac{\Xi^2-4\Xi^{1/2}+\omega_1(\Xi)+\omega_2(\Xi)-\omega_3(\Xi)-\omega_1(0)}{\nu_M\Xi^2}$
ν_{sel}	$\frac{-E_{sel}R}{2GM^2}$	$\frac{\Xi}{4}\frac{\Xi(2+\Xi)-2(1+\Xi)\ln(1+\Xi)}{[(1+\Xi)\ln(1+\Xi)-\Xi]^2}$	$\frac{9}{16}\frac{\Xi}{\nu_M^2}\int_0^\Xi F^2(\xi)\,\mathrm{d}\xi$
ν_J	$\frac{1}{\nu_M\Xi}\int_0^\Xi f(\xi)\xi^3\,\mathrm{d}\xi$	$\frac{4}{\nu_M\Xi}\left[\frac{\Xi(2+\Xi)}{1+\Xi}-2\ln(1+\Xi)\right]$	$\frac{2\Xi-\omega_1(\Xi)+\omega_2(\Xi)-\omega_3(\Xi)+\omega_1(0)}{\nu_M\Xi}$
$\omega_1(\xi)=\frac{4}{\sqrt{3}}\,\mathrm{arctg}\,\frac{2\xi^{1/2}-1}{\sqrt{3}}$; $\omega_2(\xi)=\frac{4}{3}\ln(1+\xi^{1/2})$; $\omega_3(\xi)=\frac{2}{3}\ln(1-\xi^{1/2}+\xi)$; $\omega_1(0)=\frac{-2\pi}{3\sqrt{3}}$.			

Table 1: Comparison between functions (local properties) and profile parameters (global properties), related to NFW and MOA density profiles, respectively. The profile parameters depend on a single unknown, i.e. the scaled radius, Ξ. The profile parameter, ν_J, is related to the special case of constant rotational velocity on the equatorial plane. Rigidly rotating configurations correspond to $\nu_J = \nu_I$. Caption of symbols: M - total mass within the truncation isopycnic surface; M_0 - mass of a homogeneous region with same density and boundary as the reference isopycnic surface; $\bar\rho$ - mean density within the truncation isopycnic surface; $v_{eq}(\Xi)$, $(v_0)_{eq}$ - rotational velocity with respect to the centre of mass, at a point placed on the truncation and reference isopycnic surface, respectively; I - moment of inertia; R - radius; E_{sel} - self potential-energy; G - constant of gravitation; J - angular momentum.

and the analogon for the scaling radius, r_0, reads:

$$r_0 = C_r \delta^{-1/3} \left(\frac{M}{\mathrm{M}_{10}} \right)^{2/3} \mathrm{kpc} \quad ; \tag{5a}$$

$$(C_r)_{NFW,FM} = 2\ 10^{-2/3} k_1^{-1} \quad ; \quad (C_r)_{MOA,FM} = 2\ 10^{-2/3} \quad ; \tag{5b}$$

where the normalization constant, k_1, provides a connection between NFW and MOA density profiles, in fitting the results of simulations. For further details, see FM01 and Caimmi & Marmo (2003, Appendix B).

With regard to a selected, scaled density profile (NFW or MOA), scaled parameters related to simulated haloes may be calculated via the scaling parameters, (r_0, ρ_0), defined by Eqs. (4) and (5) which, in turn, correspond to fixed choices of independent parameters, (M, δ). For sake of brevity, let us define any parameter, related to a fitting, halo, as *fitting parameter* (e.g., the mass of a fitting halo is referred to as fitting mass).

The value of the dimensionless parameter, δ, is considered to reflect an amplitude of the density perturbation at turnaround and, for this reason, it can be thought of as constant during the evolution of a halo (e.g., Cole & Lacey 1996; NFW97; FM01). From the standpoint of top-hat, spherical density perturbation, it is related to both the mass and the peak height, as shown in Appendix A.

The combination of Eqs. (4) and (5) yields:

$$\nu_M = \frac{M}{M_0} = \frac{3}{4\pi} \frac{1}{C_\rho C_r^3} \quad ; \tag{6}$$

where M_0 is the mass of a homogeneous region, with same density and boundary as the reference isopycnic surface, (r_0, ρ_0). The shape factor, ν_M, depends on the scaled radius, Ξ, as shown in Tab. 1. Then the last may be determined, with regard to a selected, fitting density profile.

Let us define a dimensionless parameter, κ, as:

$$\kappa = \delta^{1/2} \left(\frac{R}{\mathrm{kpc}} \right)^{3/2} \left(\frac{M}{\mathrm{M}_{10}} \right)^{-1} \quad ; \tag{7}$$

where $R = \Xi r_0$ is the radius of the truncation isopycnic surface. The combination of Eqs. (5) and (7) yields:

$$\kappa = C_r^{3/2} \Xi^{3/2} \quad ; \tag{8}$$

which, in turn, is related to the whole set of simulations, and depends on the fitting scaled radius, Ξ.

The simulated parameters e.g., mass, mean density, radius, of the virialized configuration, and scaled radius, shall be labeled by the index, trn, where $trn = 200, vir$, according if FM01 or KLA01 runs are involved. This is why different definitions of radius of the virialized configuration, have been used in FM01 and KLA01.

The scaling density, ρ_0, and the scaling radius, r_0, are taken as fundamental in KLA01, and then no counterpart to Eqs. (4) and (5) is provided therein. On the other hand, the results of numerical simulations (e.g., NFW97; FM01; KLA01; Bullock et al. 2001; FM03) provide additional support to the idea, that density profiles of dark matter haloes in hierarchically clustering universes have the same shape, independent of the halo mass, the initial density perturbation spectrum, and the values of cosmological parameters. Accordingly, we suppose that Eqs. (4) and (5) hold even in averaging scaled density profiles from KLA01 simulations, but different values must be assigned to the coefficients, C_ρ and C_r. In doing this, the procedure will depend on the density profile (NFW or MOA) under consideration.

With regard to NFW density profiles, the scaled radius, $\xi_{vir} = r_{vir}/r_0$, is provided for each run in KLA01, and the mean density of the virialized configuration, $\bar{\rho}_{vir} = 3M_{vir}/(4\pi r_{vir}^3)$, together with the scaling radius, r_0, may be deduced from KLA01 results. The twelve runs from KLA01 correspond to virial masses of the same order, which allows a comparison with four runs executed by FM01 i.e. $4M0$, $2M0$, $2M1$, $2M2$, where the virial masses are also of the same order.

It can be seen that the related, averaged, scaling radius is:

$$(\bar{r}_0)_{NFW,KLA} = 25.675 \text{ kpc} \quad ; \qquad (\bar{r}_0)_{NFW,FM} = 12.87 \text{ kpc} \quad ; \tag{9}$$

and the ratio equals two within the uncertainty of the results. Then we assume that the value of the constant, C_r, appearing in Eqs. (5), doubles its counterpart related to FM01 simulations, that is:

$$(C_r)_{NFW,KLA} = 4\ 10^{-2/3} k_1^{-1} \quad ; \qquad (C_r)_{MOA,KLA} = 4\ 10^{-2/3} \quad . \tag{10}$$

The parameters, M_{vir}, r_{vir}, and δ, are intrinsic to simulations (e.g., FM01) and for this reason do not depend on the fitting density profile. Accordingly, the combination of Eqs. (5a) and (10) yields:

$$(r_0)_{MOA} = k_1 (r_0)_{NFW} \quad ; \tag{11}$$

where $k_1 = 2.275$ according to Caimmi & Marmo (2003, Appendix B).

The fitting scaled radius, Ξ, is determined by averaging the results from KLA01 runs, as:

$$\Xi = (\bar{\xi}_{vir})_{NFW} = 13.50833 \quad ; \tag{12}$$

in the mass range $(0.68 - 2.10) \times 10^{12} h^{-1} \mathrm{M}_{\odot}$, which is consistent with the expected value of the lognormal distribution deduced from a statistical sample of about two thousands of dark matter haloes in the mass range $(0.5 - 1.0) \times 10^{12} h^{-1} \mathrm{M}_{\odot}$ (Bullock et al. 2001).

Then the combination of Eqs. (6) and (10) produces:

$$(C_{\rho})_{NFW,KLA} = \frac{3}{4\pi} \left[(\nu_M)_{NFW} (C_r)^3_{NFW,KLA} \right]^{-1} \quad ; \tag{13}$$

where $M = \nu_M M_0$ according to the results listed in Table 1. The combination of Eqs. (12) and (13) yields $(C_{\rho})_{NFW,KLA} = 0.209911$. Replacing the truncation radius with the virial radius, the following relation is deduced from Table 1:

$$M_{vir} = 12 M_0 \left[\ln(1 + \xi_{vir}) - \frac{\xi_{vir}}{1 + \xi_{vir}} \right] \quad ; \tag{14}$$

which allows the calculation of the scaling mass, M_0, the fitting mass, M, and then the remaining parameters, for each run in connection with NFW density profiles.

In dealing with MOA density profiles, the constant, C_r, and the scaling radius, r_0, are expressed by Eqs. (10) and (11), respectively, and the constant, C_{ρ}, takes the expression:

$$(C_{\rho})_{MOA,KLA} = \frac{2}{k_1^3} (C_{\rho})_{NFW,KLA} = \frac{75}{32\pi} (\nu_M)^{-1}_{NFW} \quad ; \tag{15}$$

where the profile parameter, ν_M, may be calculated using the results listed in Table 1 together with Eq. (12), yielding $(C_{\rho})_{MOA,KLA} = 0.0356551$. The combination of Eqs. (6), (10), and (15) produces:

$$(\nu_M)_{MOA} = \frac{1}{2} (\nu_M)_{NFW} \quad ; \tag{16}$$

which implies $(M_0)_{MOA} = 2(M_0)_{NFW}$ provided the fitting mass, M, is kept fixed passing from MOA to NFW density profiles and vice versa. To this

respect, it has already been said that the parameters, M_{vir}, r_{vir}, and δ, are also left unchanged. Then the remaining parameters may be calculated following the same procedure used in connection with FM01 simulations, as outlined in Appendix B.

3.1 Fitting, scaled dark matter haloes related to MOA and NFW density profiles

With regard to MOA density profiles, the combination of Eqs. (4b), (5b) and (6) yields:

$$\nu_M = \frac{375}{14\pi} \quad ; \tag{17}$$

and the comparison with the explicit expression of the profile factor, ν_M, listed in Table 1, produces:

$$\Xi = \left[\exp\left(\frac{375}{56\pi}\right) - 1\right]^{2/3} \quad . \tag{18}$$

With regard to NFW density profiles, similarly, we have:

$$\nu_M = \frac{375}{7\pi} \quad ; \tag{19}$$

and the comparison with the explicit expression of the profile factor, ν_M, listed in Table 1, yields:

$$\frac{1}{1+\Xi} - \ln\frac{1}{1+\Xi} = 1 + \frac{125}{28\pi} \quad . \tag{20}$$

The knowledge of the scaled radius, Ξ, via Eqs. (18) and (20), allows the calculation of the profile parameters, $\nu_{\bar{\rho}}$, ν_{eq}, ν_I, ν_{sel}, ν_J, according to the explicit expressions listed in Table 1. The related physical parameters, $\bar{\rho}$, v_{eq}, I, E_{sel}, J, may, in turn, be calculated, according to the definitions listed in Table 1 and via Eqs. (4), (5), provided the independent parameters, (M, δ), are assigned.

The scaled radius, ξ_{max}, where either NFW or MOA velocity profile, $v_{eq}(\xi)$, related to centrifugal support along a selected radial direction, attains its maximum value, may be calculated by applying the standard methods of analysis and then solving a transcendental equation.

parameter	FM01		KLA01	
	NFW	MOA	NFW	MOA
Ξ	9.20678	3.80693	13.50833	5.43586
ξ_{max}	2.16258	1.24968	2.16258	1.24968
ν_ρ	0.00417037	0.0319486	0.00140677	0.0115409
$\nu_{\bar{\rho}}$	0.0218504	0.154536	0.00848858	0.0651335
ν_M	17.05231	8.52616	20.92379	10.46189
ν_{eq}	0.893929	0.898766	0.647442	0.833159
ν_I	0.0554130	0.0892287	0.0498080	0.0799089
ν_{sel}	1.12890	0.561202	1.10549	0.632324
ν_J	0.139180	0.146741	0.128641	0.135717
ν_{rot}	0.333333	0.333333	0.333333	0.333333
κ	2.30269	2.10091	11.57498	10.13895

Table 2: Values of the scaled radius, Ξ, the scaled radius where maximum centrifugal support along a selected, radial direction occurs, ξ_{max}, the profile parameters, ν_ρ, $\nu_{\bar{\rho}}$, ν_M, ν_{eq}, ν_I, ν_{sel}, ν_J, ν_{rot}, and the dimensionless parameter, κ, related to fitting NFW and MOA density profiles, to both FM01 and KLA01 simulations. The profile parameters, ν_J and ν_{rot}, are related to the special case of constant rotational velocity on the equatorial plane. Rigidly rotating configurations correspond to $\nu_J = \nu_I$, $\nu_{rot} = \nu_I$. The profile parameter, ν_{eq}, attains values which are very close each to the other, for FM01 simulations.

Numerical values of the scaled radius, Ξ, the scaled radius where maximum centrifugal support along a selected, radial direction occurs, ξ_{max}, and the profile parameters, ν_ρ, $\nu_{\bar{\rho}}$, ν_M, ν_{eq}, ν_I, ν_{pot}, ν_J, ν_{rot}, are listed in Table 2 for fitting NFW and MOA density profiles, to both FM01 and KLA01 simulations. The profile parameter, ν_{eq}, appears to attain values which are very close each to the other, for FM01 simulations.

3.2 Deviation of simulated dark matter haloes from their fitting counterparts

The above results allow the comparison between simulated and fitting, dark matter haloes. Values of some relevant parameters related to simulations

run	m/M_{10}	z_{start}	z_{end}	N_{200}	M_{200}/M_{10}	r_{200}/kpc	δ^{-1}
$16M0$	$3.0\ 10^{-2}$	18.8	0.0	873170	$2.6\ 10^{4}$	$1.7\ 10^{3}$	1.0
$16M1$	$6.0\ 10^{-2}$	18.5	0.0	1279383	$7.8\ 10^{4}$	$2.4\ 10^{3}$	0.4
$16M2$	$6.1\ 10^{-2}$	20.4	0.0	1322351	$8.0\ 10^{4}$	$2.4\ 10^{3}$	0.6
$8M0$	$3.7\ 10^{-3}$	22.3	0.58	745735	$2.8\ 10^{3}$	$4.8\ 10^{2}$	2.5
$8M1$	$7.6\ 10^{-3}$	22.2	0.63	1186162	$9.0\ 10^{3}$	$7.2\ 10^{2}$	1.0
$8M2$	$7.6\ 10^{-3}$	23.9	0.59	1015454	$7.7\ 10^{3}$	$7.0\ 10^{2}$	3.0
$4M0$	$4.7\ 10^{-4}$	25.9	1.6	559563	$2.7\ 10^{2}$	$1.3\ 10^{2}$	10.0
$4M1$	$9.5\ 10^{-4}$	25.9	1.6	846301	$8.0\ 10^{2}$	$2.0\ 10^{2}$	3.0
$4M2$	$9.5\ 10^{-4}$	27.4	1.2	697504	$6.6\ 10^{2}$	$2.2\ 10^{2}$	6.0
$2M0$	$5.9\ 10^{-5}$	29.7	2.1	643151	$6.6\ 10^{1}$	$6.2\ 10^{1}$	35.0
$2M1$	$1.2\ 10^{-4}$	29.7	2.2	957365	$1.1\ 10^{2}$	$8.5\ 10^{1}$	12.0
$2M2$	$1.2\ 10^{-4}$	30.9	1.8	923545	$1.0\ 10^{2}$	$9.6\ 10^{1}$	30.0

Table 3: Values of some parameters related to simulated, dark matter haloes, according to FM01, for a standard CDM model with $H_0 = 50$ km s^{-1} Mpc^{-1}, $\Omega = 1$, and $\sigma_8 = 0.7$. The particle masses are equal, and the total number of particles for each simulation is $(2.0 - 2.1) \times 10^6$. Captions: m - mass of a single particle; z - redshift (at the start and end of simulation); N_{200} - total number of particles within the sphere where $\bar{\rho} = 200\rho_{crit}$ (ρ_{crit} is the critical density); M_{200} - mass enclosed within the above mentioned sphere; r_{200} - radius of the above mentioned sphere; δ - dimensionless parameter related to the amplitude of the density perturbation at the collapse. The mass unit is $\mathrm{M}_{10} = 10^{10}\mathrm{M}_{\odot}$.

with high resolution, performed by FM01, are listed in Table 3.

The framework is a standard CDM model with $H_0 = 50$ km s^{-1} Mpc^{-1}, $\Omega = 1$, and $\sigma_8 = 0.7$. The particle masses are equal, and the total number of particles for each simulation is $(2.0 - 2.1) \times 10^6$. For further details, see FM01. The ending redshift, $z_{end} > 0$, is determined so that the truncation outside the sphere did not influence the profile around r_{200}. Then the data listed in Table 3 do not make a homogeneous set, as simulations related to $z_{end} = 0$ satisfy a different condition in respect of $z_{end} > 0$. To this aim, computations related to $z_{end} = 0$ would have been continued until the above mentioned condition would be satisfied at some $z_{end} < 0$ in the future.

Values of some relevant parameters related to simulations with high res-

run	$\frac{m}{\mathrm{M}_{10}}$	z_{end}	N_{vir}	$\left(\frac{N_{vir}m}{\mathrm{M}_{10}}\right)^+$	$\left(\frac{N_{vir}m}{\mathrm{M}_{10}}\right)^-$	$\frac{M_{vir}}{\mathrm{M}_{10}}$	$\frac{r_{vir}}{\mathrm{kpc}}$	?
$A1$	$2.3\ 10^{-3}$	0	$1.2\ 10^5$	294	259	286	367	Y
$A2$	$1.9\ 10^{-2}$	0	$1.5\ 10^4$	302	268	300	373	Y
$A3$	$1.6\ 10^{-1}$	0	$1.9\ 10^3$	322	287	286	366	N
$B1$	$1.7\ 10^{-4}$	0	$1.0\ 10^6$	184	157	171	307	Y
$B2$	$1.7\ 10^{-4}$	0	$1.5\ 10^4$	2.71	2.39	157	304	N
$B3$	$1.7\ 10^{-4}$	1	$7.1\ 10^5$	125	116	121	344	Y
$C1$	$1.7\ 10^{-4}$	0	$1.1\ 10^6$	201	173	186	321	Y
$C2$	$1.1\ 10^{-2}$	0	$1.6\ 10^4$	190	163	171	314	Y
$C3$	$1.7\ 10^{-4}$	1	$5.0\ 10^5$	88	82	97	297	N
$D1$	$1.7\ 10^{-4}$	0	$1.3\ 10^6$	236	206	214	336	Y
$D2$	$1.1\ 10^{-2}$	0	$2.0\ 10^4$	236	205	214	334	Y
$D3$	$1.7\ 10^{-4}$	1	$7.9\ 10^5$	139	129	137	350	Y

Table 4: Values of some parameters related to simulated, dark matter haloes, according to KLA01, for a ΛCDM model with $H_0 = 70$ km s^{-1} Mpc^{-1}, $\Omega_0 = 1 - \Lambda_0 = 0.3$, and $\sigma_8 = 0.9$. All simulations were started at $z_{start} = 60$. Captions: m - mass of a single particle; z_{end} - redshift at the end of simulation; N_{vir} - total number of particles within the sphere where $\bar{\rho} = \rho_{crit}\Omega_0\delta_{TH}$ (ρ_{crit} is the critical density and δ_{TH} is the density excess predicted by the top-hat model); M_{vir} - total mass within the above mentioned sphere; r_{vir} - radius of the above mentioned sphere; $(N_{vir}m/\mathrm{M}_{10})^{\mp}$ - upper and lower value of $N_{vir}m/\mathrm{M}_{10}$ deduced from the data. The mass unit is $\mathrm{M}_{10} = 10^{10}\ \mathrm{M}_\odot$. A positive answer to the question mark means that the inequality, $M_{vir}^- \le M_{vir} \le M_{vir}^+$ is satisfied. The related, explicit expression, is shown by Eqs. (22).

olution, performed by KLA01, are listed in Table 4. The framework is a ΛCDM model with $H_0 = 70$ km s^{-1} Mpc^{-1}, $\Omega_0 = 1 - \Lambda_0 = 0.3$, and $\sigma_8 = 0.9$. All simulations were started at $z_{start} = 60$. The twelve runs are, in fact, three sets of simulations of only four haloes with resolution varied in each set. Thought they cannot be considered as twelve independent runs, still they may be conceived as measures of a same physical quantity, using different methods. For further details, see KLA01.

It is worth of note that the virial radius in KLA01 is not defined as the radius, r_{200}, within which the mean density is 200 times the critical density, as done by e.g., NFW97 and FM01. On the other hand, the virial radius is intended therein as the radius, r_{vir}, within which the mean density is equal to the density predicted by the top-hat model, $\bar{\rho}_{vir} = \delta_{TH}\Omega_0\rho_{crit}$, where δ_{TH} is the density excess predicted by the top-hat model and ρ_{crit} is the critical density. In the case of $\Omega_0 = 0.3$ cosmologies, it can be seen that $r_{vir} \approx 1.3 r_{200}$ (KLA01).

In general, the scaled radius, Ξ (or concentration with regard to NFW density profiles), is lowered for increasing mass (constant redshift) and redshift (constant mass). The mass range is large ($6 \cdot 10^{11} < M/\mathrm{M}_\odot \leq 8 \cdot 10^{14}$) for FM01 simulations, but the use of a CDM cosmological model makes the concentration mildly depend on the mass (at constant redshift). On the other hand, the concentration is decreased for low-mass haloes, which virialize earlier, and increased for high-mass haloes, which virialize later. The net effect is an even milder dependence of the concentration on the mass.

In any case, it can be said that the intrinsic spread in concentration is dominant over the systematic change in the mean value of the concentration on a mass bin (e.g., Bullock et al. 2001), across the entire mass ranges covered by FM01 and KLA01 simulations. Accordingly, the fitting, scaled density profile may be considered, to an acceptable extent, as related to an invariant scaled radius, Ξ.

The following inequalities may be useful for testing the intrinsic spread of some data listed in Table 3:

$$M_{200}^{-} \leq M_{200} \leq M_{200}^{+} \quad ; \quad \bar{\rho}_{200}^{-} \leq 200\rho_{crit}(z_{end}) \leq \bar{\rho}_{200}^{+} \quad ; \tag{21a}$$

$$\bar{\rho}_{200}^{-} \leq \bar{\rho}_{200} \leq \bar{\rho}_{200}^{+} \quad ; \quad \kappa_{200}^{-} \leq \kappa_{200} \leq \kappa_{200}^{+} \quad ; \tag{21b}$$

$$M_{200}^{\mp} = (N_{200} \mp \Delta N_{200})(m \mp \Delta m) \quad ; \tag{21c}$$

$$\bar{\rho}_{200}^{\mp} = \bar{\rho}_{200} \left[\frac{1 \mp \Delta M_{200}/M_{200}}{(1 \pm \Delta r_{200}/r_{200})^3} \right] \quad ; \tag{21d}$$

$$\kappa_{200}^{\mp} = (\delta \mp \Delta\delta) \frac{r_{200} \mp \Delta r_{200}}{\mathrm{kpc}} \left(\frac{M_{200}^{\pm}}{\mathrm{M}_{10}} \right)^{-1} \quad ; \tag{21e}$$

$$\bar{\rho}_{200} = \frac{3}{4\pi} \frac{M_{200}}{r_{200}^3} \quad ; \tag{21f}$$

$$\rho_{crit}(z) = 0.691785\ 10^{-8} (1+z)^3 \mathrm{M}_{10} \mathrm{kpc}^{-3} \quad ; \tag{21g}$$

$$\kappa_{200} = \delta^{1/2} \left(\frac{r_{200}}{\mathrm{kpc}} \right)^{3/2} \left(\frac{M_{200}}{\mathrm{M}_{10}} \right)^{-1} \quad ; \tag{21h}$$

where z is the redshift, $\mathrm{M}_{10} = 10^{10} \mathrm{M}_{\odot}$ and, in general, $\Delta\eta = 5 \cdot 10^{-n-1}$ is the uncertainty assumed for $\eta = u\ 10^{-n}$, $0 \leq u < 10$. Upper and lower values are listed in Table 5. A positive answer to a question mark therein, with regard to the parameter on the left of the column under consideration, means that the related inequalities, among (21a) and (21b), are satisfied, and vice versa.

Similarly, for testing the intrinsic spread of masses listed in Table 4:

$$M_{vir}^{-} \leq M_{vir} \leq M_{vir}^{+} \quad ; \tag{22a}$$

$$M_{vir}^{\mp} = (N_{vir} \mp \Delta N_{vir})(m \mp \Delta m) \quad ; \tag{22b}$$

where, in general, $\Delta\eta = 5 \cdot 10^{-n-1}$ is the uncertainty assumed for $\eta = u\ 10^{-n}$, $0 \leq u < 10$. The upper and lower values are also listed in Table 4. A positive answer to the question mark therein means that the inequality (22a) is satisfied, and vice versa.

All the data produce an acceptable intrinsic spread, with the exception of run $2M0$, in FM01, and run $B2$, in KLA01, which exhibit a substantial inconsistency in any case. The larger discrepancies can be due to nothing but printing errors. Accordingly, the value $M_{200}/\mathrm{M}_{10} = 38$, also deduced from FM01, is assigned instead of 66, to run $2M0$, and the value $m/\mathrm{M}_{10} = 1.1\ 10^{-2}$, also inferred from KLA01, is assigned instead of $1.7\ 10^{-4}$, to run $B2$.

With regard to NFW density profiles, the scaled radius, $\xi_{vir} = r_{vir}/r_0$, is provided for each run in KLA01, and the mean density of the virialized configuration, $\bar{\rho}_{vir} = 3M_{vir}/(4\pi r_{vir}^3)$, together with the scaling radius, r_0, may be deduced from the results of Table 4. The above mentioned parameters are listed in Table 6, together with two dimensionless parameters, δ and κ_{vir},

run	$\frac{M_{200}}{\mathrm{M}_{10}}$	$\left(\frac{N_{200}m}{\mathrm{M}_{10}}\right)^{+}$	$\left(\frac{N_{200}m}{\mathrm{M}_{10}}\right)^{-}$	?	κ_{200}	κ_{200}^{+}	κ_{200}^{-}	?
$16M0$	26000	26632	25758	Y	2.70	2.92	2.46	Y
$16M1$	78000	77403	76123	N	2.38	2.69	2.19	Y
$16M2$	80000	81325	80002	N	1.90	2.04	1.74	Y
$8M0$	2800	2796	2722	N	2.37	2.51	2.32	Y
$8M1$	9000	9074	8955	Y	2.15	2.24	2.06	Y
$8M2$	7700	7768	7667	Y	1.39	1.42	1.37	Y
$4M0$	270	266	260	N	1.74	1.91	1.66	Y
$4M1$	800	808	800	Y	2.04	2.14	1.93	Y
$4M2$	660	666	659	Y	2.02	2.10	1.92	Y
$2M0$	66	38	38	N	1.25	2.20	2.14	N
$2M1$	110	120	110	Y	2.06	2.08	1.86	Y
$2M2$	100	115	106	N	1.72	1.63	1.48	N

run	$\frac{200\rho_{crit}(z_{end})}{\mathrm{M}_{10}\mathrm{kpc}^{-3}}$	$\frac{\bar{\rho}_{200}^{+}}{\mathrm{M}_{10}\mathrm{kpc}^{-3}}$	$\frac{\bar{\rho}_{200}^{-}}{\mathrm{M}_{10}\mathrm{kpc}^{-3}}$	?	$\frac{\bar{\rho}_{200}}{\mathrm{M}_{10}\mathrm{kpc}^{-3}}$	?
$16M0$	$1.38\ 10^{-6}$	$1.41\ 10^{-6}$	$1.15\ 10^{-6}$	Y	$1.26\ 10^{-6}$	Y
$16M1$	$1.38\ 10^{-6}$	$1.42\ 10^{-6}$	$1.24\ 10^{-6}$	Y	$1.35\ 10^{-6}$	Y
$16M2$	$1.38\ 10^{-6}$	$1.50\ 10^{-6}$	$1.30\ 10^{-6}$	Y	$1.38\ 10^{-6}$	Y
$8M0$	$5.46\ 10^{-6}$	$6.23\ 10^{-6}$	$5.70\ 10^{-6}$	N	$6.04\ 10^{-6}$	Y
$8M1$	$5.99\ 10^{-6}$	$5.93\ 10^{-6}$	$5.61\ 10^{-6}$	N	$5.76\ 10^{-6}$	Y
$8M2$	$5.56\ 10^{-6}$	$5.52\ 10^{-6}$	$5.22\ 10^{-6}$	N	$5.36\ 10^{-6}$	Y
$4M0$	$2.43\ 10^{-5}$	$3.25\ 10^{-5}$	$2.52\ 10^{-5}$	N	$2.93\ 10^{-5}$	Y
$4M1$	$2.43\ 10^{-5}$	$2.60\ 10^{-5}$	$2.22\ 10^{-5}$	Y	$2.39\ 10^{-5}$	Y
$4M2$	$1.47\ 10^{-5}$	$1.60\ 10^{-5}$	$1.38\ 10^{-5}$	Y	$1.48\ 10^{-5}$	Y
$2M0$	$4.12\ 10^{-5}$	$3.90\ 10^{-5}$	$3.72\ 10^{-5}$	N	$6.61\ 10^{-5}$	N
$2M1$	$4.53\ 10^{-5}$	$4.75\ 10^{-5}$	$4.20\ 10^{-5}$	Y	$4.28\ 10^{-5}$	Y
$2M2$	$3.04\ 10^{-5}$	$3.15\ 10^{-5}$	$2.82\ 10^{-5}$	Y	$2.70\ 10^{-5}$	N

Table 5: Comparison between (i) the value of M_{200} and the upper and lower value of $N_{200}m$, deduced from the data listed in Table 3; (ii) the value of κ_{200} deduced from the data listed in Table 3 and the related upper and lower values, using Eqs. (21e) and (21h), respectively; and (iii) the value of $200\rho_{crit}(z_{end})$ calculated using Eq. (21g), the upper and lower value of $\bar{\rho}_{200} = 3N_{200}m/(4\pi r_{200}^3)$, and the value of $\bar{\rho}_{200} = 3M_{200}/(4\pi r_{200}^3)$, deduced from the data listed in Table 3. A positive answer to the question mark means that the related inequalities, among Eqs. (21a) and (21c), are satisfied for the values listed on the same lines of the corresponding columns. The related, explicit expressions, are shown by Eqs. (21c)-(21h) .

run	$(\xi_{vir})_{NFW}$	$\frac{(r_0)_{NFW}}{\mathrm{kpc}}$	$\frac{\bar{\rho}_{vir}}{\mathrm{M}_{10}\mathrm{kpc}^{-3}}$	δ^{-1}	κ_{vir}
$A1$	17.4	21.1	$1.38\ 10^{-6}$	2.68	16.9
$A2$	16.0	23.3	$1.38\ 10^{-6}$	3.05	14.9
$A3$	16.6	22.0	$1.39\ 10^{-6}$	2.94	15.8
$B1$	15.6	19.7	$1.41\ 10^{-6}$	5.51	14.4
$B2$	16.5	18.4	$1.33\ 10^{-6}$	5.66	15.6
$B3$	12.3	28.0	$7.10\ 10^{-7}$	25.0	10.1
$C1$	11.2	28.7	$1.33\ 10^{-6}$	10.3	8.74
$C2$	9.8	32.0	$1.32\ 10^{-6}$	14.7	7.15
$C3$	11.9	25.0	$8.84\ 10^{-7}$	26.7	9.57
$D1$	11.9	28.2	$1.35\ 10^{-6}$	7.95	9.57
$D2$	13.4	24.9	$1.37\ 10^{-6}$	6.17	11.4
$D3$	9.5	36.8	$7.64\ 10^{-7}$	33.7	6.83

Table 6: The scaled, virialized radius related to NFW density profiles, $(\xi_{vir})_{NFW}$, the scaling radius related to NFW density profiles, $(r_0)_{NFW}$, the mean density inside the virialized configuration, $\bar{\rho}_{vir}$, and the dimensionless parameters, δ^{-1} and κ_{vir}, taken from twelve runs in KLA01 or deduced from Eqs. (5), (7), and (8).

which are deduced from Eqs. (5), (7), and (8). It is apparent that the twelve runs correspond to virial masses of the same order.

At this stage, the deviation of simulated, dark matter haloes, from their fitting counterparts, may be analysed along the following steps.

(i) Select a fitting halo among NFW and MOA density profiles.

(ii) Select a simulated halo among the twelve runs in Tables 3 and 4.

(iii) Calculate the fitting mass, M, using Eqs. (4), (5), (6), and the related values of M_{trn} and r_{trn}, $trn = 200, vir$, listed in Tables 3 and 4. For a formal derivation, see Appendix B.

(iv) Calculate the values of the scaling density, ρ_0, the scaling radius, r_0, and the scaling mass, M_0. It is worth remembering the latter is the mass of a homogeneous region, with same density and boundary as the reference isopycnic surface, (r_0, ρ_0).

(v) Calculate the scaled mass, M_{trn}/M_0, the scaled radius, r_{trn}/r_0, the scaled density, $\bar{\rho}_{trn}/\rho_0$, and the dimensionless parameter, κ_{trn}, $trn = 200, vir$.

(vi) Return to (ii).

(vii) Return to (i).

Simulated haloes may be characterized by four scaled parameters, M_{trn}/M_0, r_{trn}/r_0, $\bar{\rho}_{trn}/\bar{\rho}_0$, and κ_{trn}. Their fitting counterparts are ν_M, Ξ, $\nu_{\bar{\rho}}$, and κ, respectively, which have been listed in Table 2. The fitting mass, M, the scaling density, radius, mass, ρ_0, r_0, M_0, and the ratios of three parameters related to simulated haloes, to their fitting counterparts, κ_{trn}/κ, M_{trn}/M, r_{trn}/R, are listed in Tables 7 and 8, in connection with both NFW and MOA density profiles, for the twelwe runs from FM01 and KLA01, respectively.

4 Discussion.

The deviation of simulated dark matter haloes from their fitting counterparts, can be seen in Figs. 1, 2, 3, 4, and in Figs. 5, 6, 7, 8, in connection with

run	$\frac{M}{\mathrm{M}_{10}}$	$\frac{\rho_0}{\mathrm{M}_{10}\mathrm{kpc}^{-3}}$	$\frac{r_0}{\mathrm{kpc}}$	$\frac{M_0}{\mathrm{M}_{10}}$	$\frac{\kappa_{200}}{\kappa}$	$\frac{M_{200}}{M}$	$\frac{r_{200}}{R}$
			NFW				
$16M0$	$2.37\ 10^4$	$8.69\ 10^{-5}$	$1.56\ 10^2$	$1.39\ 10^3$	1.17	1.10	1.18
$16M1$	$7.64\ 10^4$	$6.74\ 10^{-5}$	$2.51\ 10^2$	$4.48\ 10^3$	1.03	1.02	1.04
$16M2$	$9.09\ 10^4$	$3.78\ 10^{-5}$	$3.23\ 10^2$	$5.33\ 10^3$	0.824	0.880	0.807
$8M0$	$2.75\ 10^3$	$3.00\ 10^{-4}$	$5.04\ 10^1$	$1.61\ 10^2$	1.03	1.02	1.03
$8M1$	$9.41\ 10^3$	$2.19\ 10^{-4}$	$8.44\ 10^1$	$5.52\ 10^2$	0.932	0.957	0.926
$8M2$	$1.24\ 10^4$	$6.11\ 10^{-5}$	$1.37\ 10^2$	$6.59\ 10^2$	0.603	0.685	0.554
$4M0$	$3.27\ 10^2$	$6.29\ 10^{-4}$	$1.94\ 10^1$	$1.92\ 10^1$	0.754	0.825	0.728
$4M1$	$8.64\ 10^2$	$7.94\ 10^{-4}$	$2.49\ 10^1$	$5.07\ 10^1$	0.886	0.925	0.876
$4M2$	$7.19\ 10^2$	$4.78\ 10^{-4}$	$2.76\ 10^1$	$4.21\ 10^1$	0.877	0.918	0.865
$2M0$	$3.94\ 10^1$	$1.49\ 10^{-3}$	$7.18\ 10^0$	$2.31\ 10^0$	0.943	0.964	0.938
$2M1$	$1.18\ 10^2$	$1.45\ 10^{-3}$	$1.04\ 10^1$	$6.94\ 10^0$	0.893	0.930	0.884
$2M2$	$1.22\ 10^2$	$5.62\ 10^{-4}$	$1.45\ 10^1$	$7.17\ 10^0$	0.746	0.818	0.719
			MOA				
$16M0$	$2.22\ 10^4$	$1.58\ 10^{-5}$	$3.40\ 10^2$	$2.60\ 10^3$	1.28	1.17	1.31
$16M1$	$7.17\ 10^4$	$1.22\ 10^{-5}$	$5.48\ 10^2$	$8.41\ 10^3$	1.13	1.09	1.15
$16M2$	$8.62\ 10^4$	$6.76\ 10^{-6}$	$7.09\ 10^2$	$1.01\ 10^4$	0.903	0.928	0.889
$8M0$	$2.58\ 10^3$	$5.43\ 10^{-5}$	$1.10\ 10^2$	$3.03\ 10^2$	1.13	1.09	1.15
$8M1$	$8.87\ 10^3$	$3.55\ 10^{-5}$	$1.85\ 10^2$	$1.05\ 10^3$	1.02	1.01	1.02
$8M2$	$1.10\ 10^4$	$1.06\ 10^{-5}$	$3.08\ 10^2$	$1.30\ 10^3$	0.661	0.698	0.597
$4M0$	$3.13\ 10^2$	$1.12\ 10^{-4}$	$4.28\ 10^1$	$3.68\ 10^1$	0.826	0.863	0.798
$4M1$	$8.17\ 10^2$	$1.43\ 10^{-4}$	$5.43\ 10^1$	$9.59\ 10^1$	0.972	0.980	0.968
$4M2$	$6.79\ 10^2$	$8.59\ 10^{-5}$	$6.05\ 10^1$	$7.97\ 10^1$	0.961	0.972	0.955
$2M0$	$3.71\ 10^1$	$8.60\ 10^{-6}$	$1.57\ 10^1$	$4.36\ 10^0$	1.03	1.02	1.04
$2M1$	$1.12\ 10^2$	$2.61\ 10^{-4}$	$2.29\ 10^1$	$1.31\ 10^1$	0.979	0.985	0.976
$2M2$	$1.17\ 10^2$	$9.98\ 10^{-5}$	$3.20\ 10^1$	$1.37\ 10^1$	0.817	0.856	0.788

Table 7: The fitting mass, M, the scaling density, radius, mass, ρ_0, r_0, M_0, and the ratios of three parameters related to simulated haloes to their fitting counterparts, κ_{200}/κ, M_{200}/M, r_{200}/R, in connection with NFW and MOA density profiles, and twelve runs from FM01.

run	$\frac{M}{\mathrm{M}_{10}}$	$\frac{\rho_0}{\mathrm{M}_{10}\mathrm{kpc}^{-3}}$	$\frac{M_0}{\mathrm{M}_{10}}$	$\frac{\kappa_{vir}}{\kappa}$	$\frac{M_{vir}}{M}$	$\frac{r_{vir}}{R}$
		NFW				
$A1$	254	$3.08\ 10^{-4}$	12.1	1.46	1.13	1.29
$A2$	276	$2.49\ 10^{-4}$	13.2	1.29	1.08	1.18
$A3$	259	$2.76\ 10^{-4}$	12.4	1.36	1.10	1.23
$B1$	159	$2.39\ 10^{-4}$	7.62	1.24	1.07	1.15
$B2$	143	$2.60\ 10^{-4}$	6.82	1.35	1.10	1.22
$B3$	127	$6.62\ 10^{-5}$	6.06	0.869	0.954	0.910
$C1$	205	$9.93\ 10^{-5}$	9.79	0.755	0.908	0.829
$C2$	202	$7.02\ 10^{-5}$	9.68	0.618	0.844	0.725
$C3$	103	$7.59\ 10^{-5}$	4.94	0.827	0.937	0.881
$D1$	228	$1.16\ 10^{-4}$	10.9	0.827	0.937	0.881
$D2$	215	$1.58\ 10^{-4}$	10.3	0.988	0.996	0.992
$D3$	165	$3.77\ 10^{-5}$	7.89	0.590	0.830	0.703
		MOA				
$A1$	236	$5.63\ 10^{-5}$	22.6	1.48	1.21	1.48
$A2$	258	$4.54\ 10^{-5}$	24.6	1.36	1.16	1.36
$A3$	241	$5.02\ 10^{-5}$	23.1	1.41	1.18	1.41
$B1$	149	$4.35\ 10^{-5}$	14.2	1.32	1.15	1.32
$B2$	133	$4.74\ 10^{-5}$	12.7	1.40	1.18	1.40
$B3$	118	$1.20\ 10^{-5}$	11.3	1.04	1.02	1.04
$C1$	191	$1.81\ 10^{-5}$	18.3	0.950	0.972	0.948
$C2$	190	$1.28\ 10^{-5}$	18.1	0.837	0.901	0.829
$C3$	96.6	$1.38\ 10^{-5}$	9.23	1.01	1.00	1.01
$D1$	213	$2.10\ 10^{-5}$	20.4	1.01	1.00	1.01
$D2$	200	$2.88\ 10^{-5}$	19.2	1.13	1.07	1.13
$D3$	155	$6.83\ 10^{-6}$	14.8	0.812	0.884	0.802

Table 8: The fitting mass, M, the scaling density and mass, ρ_0, and M_0, and the ratios of three parameters related to simulated haloes, to their fitting counterparts, κ_{vir}/κ, M_{vir}/M, r_{vir}/R, in connection with NFW and MOA density profiles, and twelve runs from KLA01.

FM01 and KLA01 simulations, respectively. The following plots are represented: scaled mass, M_{trn}/M_0, vs. logarithmic scaled mass, $\log(M_{trn}/\mathrm{M}_{10})$; scaled radius, r_{trn}/r_0, vs. logarithmic scaled radius, $\log(r_{trn}/\mathrm{kpc})$; scaled density, $\bar{\rho}_{trn}/\rho_0$, vs. logarithmic scaled density, $\log[\bar{\rho}_{trn}/(\mathrm{M}_{10}\mathrm{kpc}^{-3})]$; and dimensionless parameter, κ_{trn}, vs. logarithmic scaled mass, $\log(M_{trn}/\mathrm{M}_{10})$; where $tnr = 200, vir$. The deviation of the above mentioned, scaled parameters, from their fitting counterparts, are clearly shown therein.

The mean value, $\bar{\eta}$, the standard deviation from the mean value, $\sigma_{s\bar{\eta}}$, and the standard deviation from the standard deviation from the mean value, $\sigma_{s\bar{\mu}}$, which are expressed as (e.g., Oliva & Terrasi 1976, Chap. V, § 5.6.3):

$$\bar{\eta} = \frac{1}{n}\sum_{i=1}^{n}\eta_i \quad ; \tag{23}$$

$$\sigma_{s\bar{\eta}} = \left[\frac{1}{n}\frac{1}{n-1}\sum_{i=1}^{n}(\eta_i - \bar{\eta})^2\right]^{1/2} \quad ; \tag{24}$$

$$\sigma_{s\bar{\mu}} = \frac{\sigma_{s\bar{\eta}}}{\sqrt{2n}} \quad ; \quad \bar{\mu} = \sigma_{s\bar{\eta}} \quad ; \tag{25}$$

where $n = 12$; $\eta = M_{trn}/M_0$, r_{trn}/r_0, $\bar{\rho}_{trn}/\rho_0$, κ_{trn}; $tnr = 200, vir$; and $\bar{\eta}$, $\sigma_{s\bar{\eta}}$, $\sigma_{s\bar{\mu}}$, are shown by the vertical bars on Figs. 1-8.

Numerical values of $\bar{\eta}$, $\sigma_{s\bar{\eta}}$, $\sigma_{s\bar{\mu}}$, deduced by Eqs. (23), (24), and (25), respectively, are listed in Table 9, together with their fitting counterparts, η^*, which have been represented as horizontal lines in Figs. 1-8 and listed in Table 2, in connection with NFW and MOA density profiles. It is apparent that the following inequalities hold:

$$\bar{\eta} - u\sigma_{s\bar{\eta}} - u\sigma_{s\bar{\mu}} < \eta^* < \bar{\eta} + u\sigma_{s\bar{\eta}} + u\sigma_{s\bar{\mu}} \quad ; \tag{26}$$

where $u = 2, 1$ for NFW and MOA density profiles, respectively, in connection with FM01 simulations, and the contrary holds, in connection with KLA01 simulations. Then the best fitting density profile (among NFW and MOA in the case under discussion) may be chosen as minimizing the ratio, $|x_{\overline{\eta}}|/\sigma_{s\,\overline{\eta}} = |\overline{\eta} - \eta^*|/\sigma_{s\,\overline{\eta}}$, for the scaled parameter of interest.

It can also be shown that a necessary condition for the detectability of accidental errors, $\Delta\eta \leq \sigma_\eta$, is satisfied for any choice of η listed in Table 9. More specifically, $\Delta\eta$ and σ_η represent the sensitivity error of the simulation and the rms error, respectively, with regard to η. For a formal demonstration, see Appendix C.

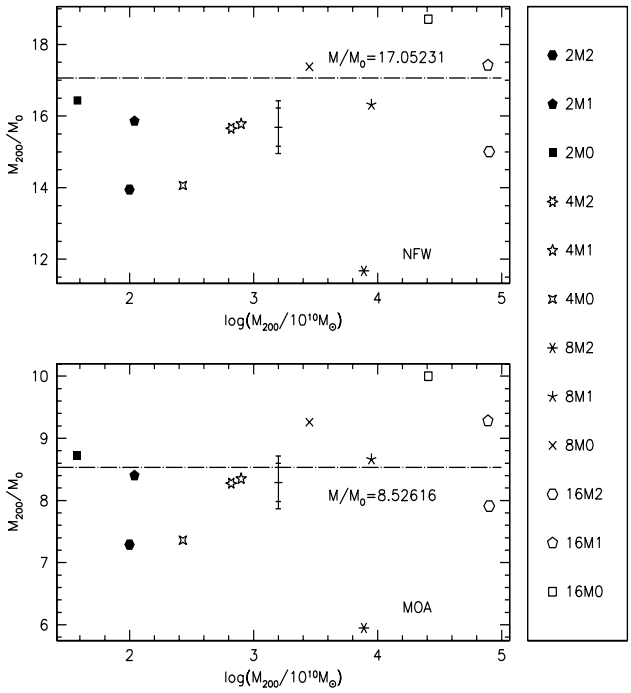

Figure 1: Deviation of simulated dark matter haloes from their fitting counterparts, with regard to the scaled, virial mass, M_{200}/M_0, for both NFW (top) and MOA (bottom) density profiles. Fitting haloes lie on the horizontal line, while simulated haloes are represented by different symbols. The vertical bar is centred on the mean value of plotted data, with respect to the ordinates (and no connection with the abscissae), and is limited by the standard deviation from the mean, without (inner boundary) and with (outer boundary) addition of about twice the standard deviation from the standard deviation from the mean, deduced from Eqs. (23), (24), and (25), respectively. Captions of symbols on the right correspond to FM01 runs listed in Tables 3, 5, and 7.

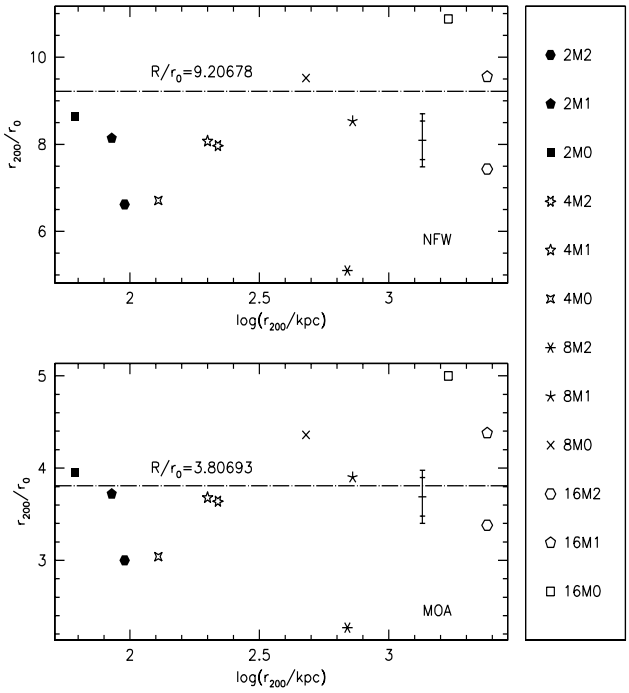

Figure 2: Deviation of simulated dark matter haloes from their fitting counterparts, with regard to the scaled radius, r_{200}/r_0, for both NFW (top) and MOA (bottom) self-similar, universal density profiles. Other captions as in Fig. 1.

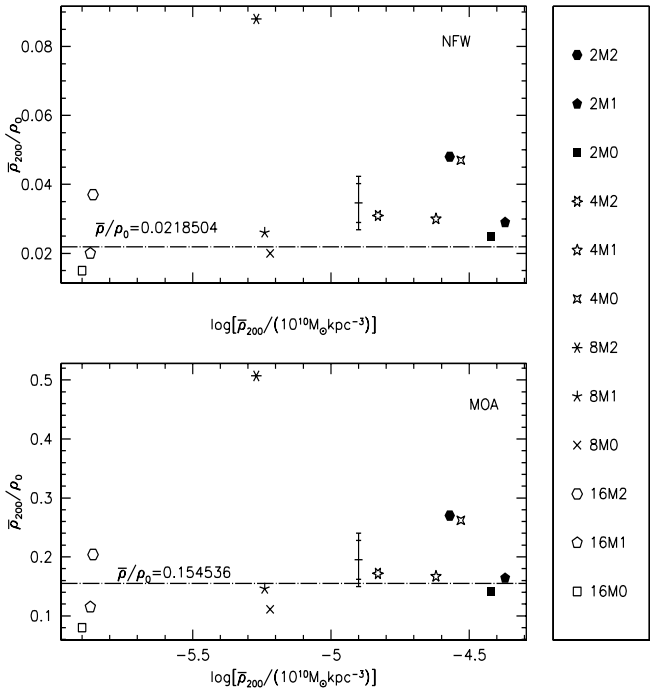

Figure 3: Deviation of simulated dark matter haloes from their fitting counterparts, with regard to the scaled density, $\bar{\rho}_{200}/\rho_0$, for both NFW (top) and MOA (bottom) self-similar, universal density profiles. Other captions as in Fig. 1.

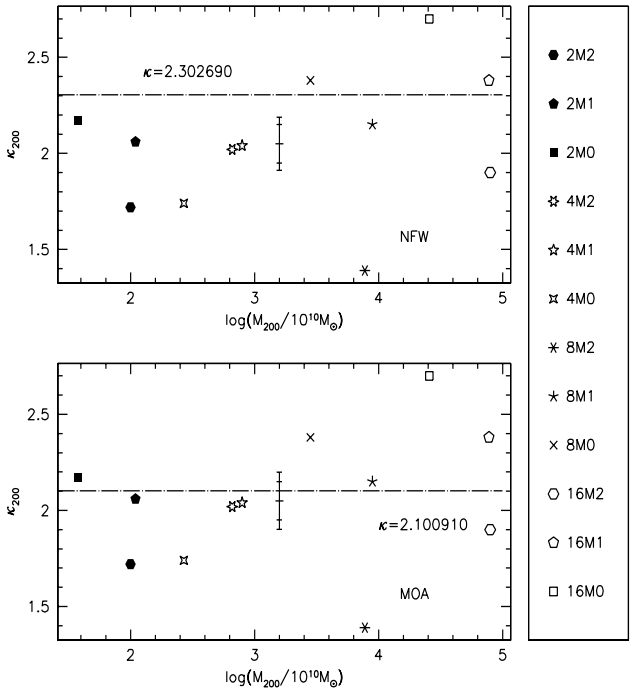

Figure 4: Deviation of simulated dark matter haloes from their fitting counterparts, with regard to the dimensionless parameter, κ_{200}, for both NFW (top) and MOA (bottom) self-similar, universal density profiles. Other captions as in Fig. 1.

parameter	NFW				MOA			
η	$\bar{\eta}$	$\sigma_{s\bar{\eta}}$	$\sigma_{s\bar{\mu}}$	η^*	$\bar{\eta}$	$\sigma_{s\bar{\eta}}$	$\sigma_{s\bar{\mu}}$	η^*
M_{200}/M_0	15.69	0.538	0.110	17.05	8.29	0.309	0.0630	8.53
r_{200}/r_0	8.09	0.443	0.0902	9.21	3.69	0.209	0.0427	3.81
$\bar{\rho}_{200}/\rho_0$	0.0346	0.00564	0.00115	0.0218	0.195	0.0328	0.00669	0.154
κ_{200}	2.05	0.100	0.0205	2.30	2.05	0.100	0.0205	2.10
M_{vir}/M_0	20.74	0.632	0.129	20.92	11.11	0.343	0.0701	10.46
r_{vir}/r_0	13.51	0.807	0.165	13.51	5.94	0.355	0.0723	5.44
$\bar{\rho}_{vir}/\rho_0$	0.0101	0.00155	0.000317	0.00849	0.0556	0.00855	0.00174	0.0651
κ_{vir}	11.75	1.03	0.211	11.57	11.75	1.03	0.211	10.14

Table 9: The mean value, $\bar{\eta}$, the standard deviation from the mean value, $\sigma_{s\bar{\eta}}$, and the standard deviation from the standard deviation from the mean value, $\sigma_{s\bar{\mu}}$, where $\eta = M_{trn}/M_0$, r_{trn}/r_0, $\bar{\rho}_{trn}/\rho_0$, κ_{trn}, $trn = 200, vir$, deduced from simulated haloes, data from Tables 3, 5, 7 (FM01), and 4, 6, 8 (KLA01). The value of the related fitting counterparts, $\eta^* = \nu_M$, Ξ, $\nu_{\bar{\rho}}$, κ, listed in Table 2, is also reported for comparison. The upper and lower panel are related to FM01 and KLA01 simulations, respectively. The left-hand and right-hand side are related to NFW and MOA universal density profiles, respectively.

It is apparent that NFW density profiles reproduce FM01 simulations to a lesser extent with respect to MOA density profiles, while the contrary holds with regard to KLA01 simulations, according to the above mentioned criterion. In any case, a better fit could be obtained by use of a different scaled density profile, i.e. different values of the exponents, (α, β, γ), appearing in Eq. (1).

4.1 Standard deviations deduced from the propagation of the errors

Universal density profiles, expressed by Eq. (1), are currently used in fitting simulated density profiles (e.g., NFW; FM01; FM03). The choice of the exponents, (α, β, γ), allows the scaled parameters, $\nu_M = M/M_0$, $\nu_{\bar{\rho}} = \bar{\rho}/\rho_0$, and k, depend on a single scaled parameter i.e. the scaled radius, Ξ, or concentration with regard to NFW density profiles. As the concentration exhibits a lognormal distribution (e.g., Bullock et al. 2001), and the above mentioned parameters may be considered as depending on the decimal logarithm of the concentration, $\log \Xi$, the related distribution is expected to be (at least to a first extent) normal, via the same procedure which leads to the propagation of the errors.

The corresponding rms errors are:

$$\sigma_{\Xi} = \Xi \sigma_{\log \Xi} \quad ; \tag{27}$$

$$\sigma_{\nu_M} = 3 f(\Xi) \Xi^3 \sigma_{\log \Xi} \quad ; \tag{28}$$

$$\sigma_{\nu_{\bar{\rho}}} = 3 \left| f(\Xi) - \frac{1}{\Xi^3} \frac{M}{M_0} \right| \sigma_{\log \Xi} \quad ; \tag{29}$$

$$\sigma_k = \frac{3}{2} k \sigma_{\log \Xi} \quad ; \tag{30}$$

where $f(\Xi)$ is the scaled density, expressed by Eq. (2), particularized to the scaled radius, $\xi = \Xi$. For a formal demonstration, see Appendix D.

A comparison between rms errors, expressed by the above relations, and standard deviations, listed in Table 9, needs the following steps.

(a) Assume a rms error of the lognormal distribution of the concentration as in Bullock el al. (2001), $\sigma_{\log \Xi} = 0.18$.

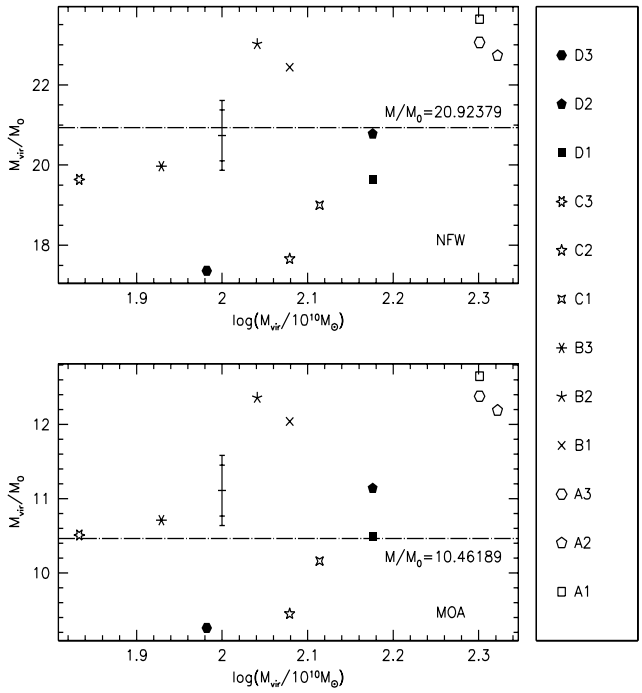

Figure 5: Deviation of simulated dark matter haloes from their fitting counterparts, with regard to the scaled virial mass, M_{vir}/M_0, for both NFW (top) and MOA (bottom) self-similar, universal density profiles. Fitting haloes lie on the horizontal line, while simulated haloes are represented by different symbols. The vertical bar is centred on the mean value of plotted data, with respect to the ordinates (and no connection with the abscissae), and is limited by the standard deviation of the mean, without (inner boundary) and with (outer boundary) addition of about twice the standard deviation from the standard deviation from the mean, deduced from Eqs. (23), (24), and (25), respectively. Captions of symbols on the right correspond to KLA01 runs listed in Tables 4, 6, and 8.

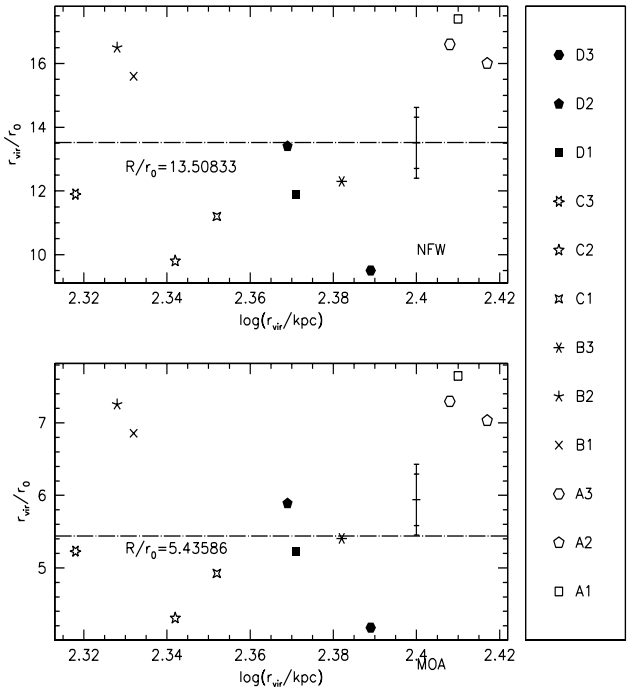

Figure 6: Deviation of simulated dark matter haloes from their fitting counterparts, with regard to the scaled radius, r_{vir}/r_0, for both NFW (top) and MOA (bottom) self-similar, universal density profiles. Other captions as in Fig. 5.

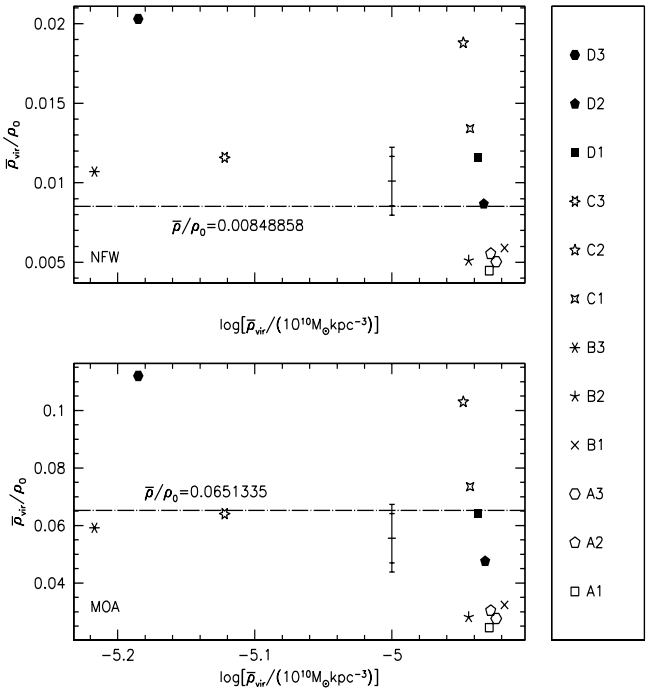

Figure 7: Deviation of simulated dark matter haloes from their fitting counterparts, with regard to the scaled density, $\bar{\rho}_{vir}/\rho_0$, for both NFW (top) and MOA (bottom) self-similar, universal density profiles. Other captions as in Fig. 5.

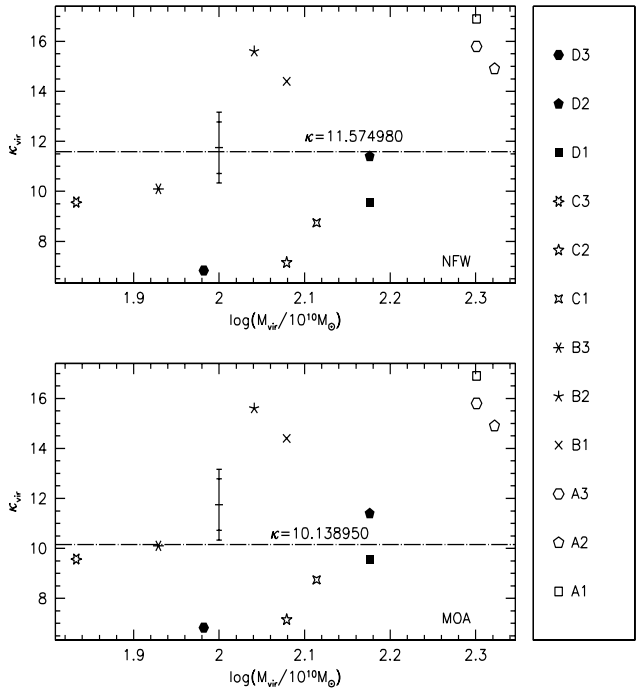

Figure 8: Deviation of simulated dark matter haloes from their fitting counterparts, with regard to the dimensionless parameter, κ_{vir}, for both NFW (top) and MOA (bottom) self-similar, universal density profiles. Other captions as in Fig. 5.

parameter	NFW				MOA			
η	$\sigma_{\bar{\eta}}$	$\sigma_{\bar{\eta}}/\eta^*$	$\lvert x_{\bar{\eta}}\rvert$	$\lvert x_{\bar{\eta}}\rvert/\sigma_{\bar{\eta}}$	$\sigma_{\bar{\eta}}$	$\sigma_{\bar{\eta}}/\eta^*$	$\lvert x_{\bar{\eta}}\rvert$	$\lvert x_{\bar{\eta}}\rvert/\sigma_{\bar{\eta}}$
M_{200}/M_0	1.17	0.0685	1.36	1.16	0.633	0.0742	0.24	0.379
r_{200}/r_0	1.10	0.120	1.12	1.02	0.455	0.120	0.12	0.264
$\bar{\rho}_{200}/\rho_0$	0.0635	0.290	0.0128	2.02	0.0440	0.285	0.041	0.932
κ_{200}	0.413	0.179	0.25	0.605	0.377	0.179	0.05	0.133
M_{vir}/M_0	1.24	0.0595	0.18	0.145	0.665	0.0636	0.65	0.977
r_{vir}/r_0	1.62	0.120	0	0	0.650	0.120	0.5	0.769
$\bar{\rho}_{vir}/\rho_0$	0.00254	0.299	0.00161	0.634	0.0192	0.295	0.0095	0.495
κ_{vir}	2.30	0.179	0.18	0.0783	1.82	0.179	1.61	0.885

Table 10: The rms errors, $\sigma_{\bar{\eta}}$, the ratios of rms error to the expected value of the related distribution, $\sigma_{\bar{\eta}}/\eta^*$, the absolute errors, $|x_{\bar{\eta}}| = |\bar{\eta} - \eta^*|$, and the ratios of absolute error to rms error, $|x_{\bar{\eta}}|/\sigma_{\bar{\eta}}$, where $\eta = M_{trn}/M_0$, r_{trn}/r_0, $\bar{\rho}_{trn}/\rho_0$, κ_{trn}, $trn = 200, vir$, deduced from simulated haloes, data from Tables 3, 5, 7 (FM01), and 4, 6, 8 (KLA01). Values of parameters related to their fitting counterparts, $\eta^* = \nu_M$, Ξ, $\nu_{\bar{\rho}}$, κ, are taken from Table 2. The upper and lower panel are related to FM01 and KLA01 simulations, respectively. The left-hand and right-hand side are related to NFW and MOA density profiles, respectively.

(b) Assume a scaled radius related to the expected value of the lognormal distribution of the concentration, $\Xi^* = \exp_{10}(\log \Xi)^*$, as listed in Table 9 for each universal density profile and each set of simulations.

(c) Divide the rms errors, σ_η, $\eta = \Xi,\ \nu_M,\ \nu_{\bar{\rho}},\ k$, by the square root of the number of measures that have been averaged in calculating the standard deviations from the mean, which is equal to $\sqrt{12}$.

(d) For a selected, universal density profile and a selected set of simulations, use the mean values, $\overline{\eta}$, and their fitting counterparts, η^*, listed in Table 9.

The rms errors, $\sigma_{\bar{\eta}}$, and the ratios of rms error to the expected value of the related distribution, $\sigma_{\bar{\eta}}/\eta^*$, the absolute errors, $|x_{\bar{\eta}}| = |\bar{\eta} - \eta^*|$, and the ratios of absolute error to rms error, $|x_{\bar{\eta}}|/\sigma_{\bar{\eta}}$, are listed in Table 10 with regard to FM01 (upper panel) and KLA01 (lower panel) simulations, related to NFW (left-hand side) and MOA (right-hand side) universal density profiles.

The rms errors appear to be systematically larger than the related standard deviations listed in Table 9, essentially for three orders of reasons. First, the statistical significance of the samples considered is low, owing to the small number of objects ($N = 12$). In addition, KLA01 runs make in fact three sets of simulations of only four dark matter haloes with resolution varied in each set. For this reason, they cannot be treated as twelve independent runs, and a lower standard deviation is expected.

Second, the rms errors calculated by use of Eqs. (27)-(30) need a normal distribution for the related random variables, which holds to a good extent only if the fluctuations are sufficiently small, to neglect higher-order terms, with respect to the first, in the related series developments. For further details, see Appendix D.

Third, the comparison between rms errors and standard deviations should be valid only in connection with the cosmological model, and the universal density profile, used by Bullock et al. (2001) in building up the statistical sample of simulated dark matter haloes, from which a lognormal distribution of the concentration has been deduced, with rms error $\sigma_{\log \Xi_{trn}} = 0.18$. It needs $\Lambda_0 = 0.7$, $\Omega_0 = 0.3$, $h = 0.7$, $\sigma_8 = 1.0$, and a NFW density profile. In fact, larger discrepancies occur for FM01 simulations, where $\Lambda_0 = 0$, $\Omega_0 = 1$, $h = 0.5$, and $\sigma_8 = 0.7$. On the other hand, KLA01 simulations were performed with the same choice of cosmological parameters as in Bullock et al. (2001), with the exception of $\sigma_8 = 0.9$. Then we expect that a lognormal distribution of concentration for an assigned mass bin occurs for any plausible choice of cosmological parameters, and its expected value and rms error do not change dramatically for any plausible variation of cosmological parameters.

The existence of a lognormal distribution is a necessary, but not sufficient condition, for the validity of the central limit theorem. In this view, the concentration is related to the final properties of a simulated halo, which are connected with the initial conditions, α_1, α_2, ..., α_n, by a transformation, $\Xi = \alpha_1 \alpha_2 ... \alpha_n$, as in dealing with the process of star formation, where the stellar mass follows a lognormal distribution (Adams & Fatuzzo 1996; Padoan et al. 1997). With regard to dark matter haloes within a fixed mass bin, an interpretation of the lognormal distribution, depending on the concentration, in terms of the central limit theorem, is outlined in Appendix E.

It is worth recalling that standard deviations of scaled parameters from their mean values, have been deduced directly from the results of simula-

tions, with regard to a selected, fitting density profile. On the other hand, rms errors of scaled parameters have been deduced from their dependence on the (decimal) logarithm of the concentration, $\log \Xi$, and the lognormal distribution of the concentration.

An inspection to Table 10 shows that the ratio of absolute error to rms error, is closer to zero for MOA density profiles with regard to FM01 simulations, and for NFW density profiles with regard to KLA01 simulations. This agrees with the results found using standard deviations from the mean, represented in Figs. 1-8, which have been deduced directly from simulations, with regard to a selected, fitting density profile. Then a valid criterion for the choice of a fitting density profile, in connection with a given set of simulated, dark matter haloes, appears to be the following.

Statistic razor for fitting density profiles to simulated, dark matter haloes *Given two or more fitting density profiles and a set of simulated haloes, the best fit is related to the minimum value of the ratio of the absolute error to the corresponding standard deviation from the mean,* $|x_{\overline{\eta}}|/\sigma_{s\,\overline{\eta}} = |\overline{\eta} - \eta^*|/\sigma_{s\,\overline{\eta}}$.

4.2 Interpretation in terms of the spherical top-hat model

The spherical, top-hat model makes a valid reference for simulated haloes (e.g., Cole & Lacey 1996; KLA01), and for this reason we think an interpretation of the dimensionless parameter, δ, in terms of the spherical top-hat model, may be of some utility. With regard to fitting, dark matter haloes, the combination of Eqs. (5a), (7), and (8) yields:

$$\delta = \frac{4\pi}{3} C_r^3 \Xi^3 \frac{\bar{\rho}}{\mathrm{M_{10}kpc^{-3}}} \frac{M}{\mathrm{M_{10}}} \quad ; \tag{31}$$

which shows the dependence of δ on the product, $\bar{\rho}M$.

With regard to FM01 simulations, an inspection of Table 3 shows that while the mean density, $\bar{\rho}_{200}$, is inversely proportional to the (fiducial) total mass, M_{200}, the dimensionless parameter, δ, is directly proportional to M_{200}. It can also be seen that the product, $\bar{\rho}_{200} M_{200}$, also increases as M_{200} does and vice versa, in agreement with Eq. (31). The parameter, δ, appears to depend on the mass, M, and a second independent parameter, which may

be chosen as the mass excess at the start of simulation, $(\delta M/M)_{start}$, or the related mean peak height, $\bar{\nu}_{start} = (\delta M/M)_{start}/ < (\delta M/M)^2_{start} >^{1/2}$.

In the framework of the spherical, top-hat model, the total mass is conserved and the following relations hold:

$$\frac{\bar{\rho}_{vir}}{\bar{\rho}_{max}} = \frac{R^3_{max}}{R^3_{vir}} \quad ; \qquad \frac{\bar{\rho}_{max}}{\bar{\rho}_{rec}} = \frac{R^3_{rec}}{R^3_{max}} \quad ; \tag{32}$$

where the indices, rec, max, vir, denote recombination, maximum expansion, virialization, respectively, and the ratio, $(R_{rec}/R_{max})^{-1}$, is a solution of the third-degree equation:

$$\Lambda_{rec} x^3 + \left\{ 1 - \Omega_{rec} \left[1 + \left(\frac{\delta M^*}{M} \right)_{rec} \right] - \Lambda_{rec} \right\} x + \Omega_{rec} \left[1 + \left(\frac{\delta M^*}{M} \right)_{rec} \right] = 0 \quad ; \tag{33}$$

where Ω and Λ represent the density parameter related to matter and cosmological constant, respectively, and $\delta M^*/M$ is the mean mass excess within a spherical volume where the mass of the material Hubble flow equals M (e.g., Lokas & Hoffman 2001a,b).

The solution to Eq. (33) which is of interest here, in absence of cosmological constant i.e. $\Lambda \to 0$, has to attain the limiting expression (e.g., Peebles 1980, Chap. II, §19a):

$$\frac{R_{rec}}{(R_{max})_{\Lambda=0}} = \frac{1 - \Omega^{-1}_{rec} + (\delta M^*/M)_{rec}}{1 + (\delta M^*/M)_{rec}} \approx \left(\frac{\delta M^*}{M} \right)_{rec} \quad ;$$
$$|1 - \Omega^{-1}_{rec}| \ll \left(\frac{\delta M^*}{M} \right)_{rec} \ll 1 \quad ; \tag{34}$$

where the mass excess, at recombination epoch, has a substantial contribution from both the growing and the decreasing mode of the density perturbation. For further details see e.g., Caimmi et al. (1990).

The combination of Eqs. (32) and (34) yields:

$$\frac{\bar{\rho}_{max}}{\bar{\rho}_{rec}} = \zeta_{max} \left[\left(\frac{\delta M^*}{M} \right)_{rec} \right]^3 ; \; \zeta_{max} = \left[\frac{(R_{max})_{\Lambda=0}}{R_{max}} \right]^3 ; \; |1 - \Omega^{-1}_{rec}| \ll \left(\frac{\delta M^*}{M} \right)_{rec} \ll 1; \tag{35}$$

and, in addition:

$$\frac{\bar{\rho}_{vir}}{\bar{\rho}_{max}} = \zeta_{vir} \quad ; \qquad 1 \leq \zeta_{vir} \leq 8 \quad ; \tag{36}$$

where the upper limit corresponds to null kinetic energy at maximum expansion, and the lower limit is related to a necessary condition for maximum expansion, $R_{vir} \leq R_{max}$. For further details see e.g., Caimmi et al. (1990). Finally, the combination of Eqs. (32), (35), and (36), produces:

$$\bar{\rho}_{vir} = \zeta_{max}\zeta_{vir}(\rho_h)_{rec}\left[\left(\frac{\delta M^*}{M}\right)_{rec}\right]^3 \quad ; \qquad |1-\Omega_{rec}^{-1}| \ll \left(\frac{\delta M^*}{M}\right)_{rec} \ll 1 \quad ; \tag{37}$$

where $(\rho_h)_{rec} = \bar{\rho}_{rec}/[1 + (\delta M^*/M)_{rec}]$ is the density of the material Hubble flow at recombination epoch. The above relation may be cast under the equivalent form:

$$\bar{\rho}_{vir} = \frac{125}{72\pi}\zeta_{max}\zeta_{vir}\frac{H_0^2\Omega_0}{G}\left[\left(\frac{\delta M}{M}\right)_0\right]^3 \quad ; \qquad |1-\Omega_{rec}^{-1}| \ll \left(\frac{\delta M^*}{M}\right)_{rec} \ll 1 \quad ; \tag{38}$$

where $(\delta M/M)_0 = (3/5)(\delta M^*/M)_{rec}(1 + z_{rec})$ represents the present-day mass excess of the growing mode predicted by the top-hat model, in a flat cosmology with a vanishing quintessence or, in particular, cosmological constant. For a formal derivation, see Appendix A.

The combination of Eqs. (31) and (38) yields:

$$\delta = C_\delta \zeta_{max}\left[\left(\frac{\delta M}{M}\right)_0\right]^3 \frac{M}{\mathrm{M}_{10}} \quad ; \tag{39a}$$

$$C_\delta = \frac{125}{54}\zeta_{vir}C_r^3\Xi^3\frac{H_0^2\Omega_0}{G}\frac{\mathrm{kpc}^3}{\mathrm{M}_{10}} \quad ; \qquad |1-\Omega_{rec}^{-1}| \ll 1 \quad ; \tag{39b}$$

where the coefficient, C_δ, may be evaluated numerically by use of Eqs. (5b), (10), and (36), taking the value of the scaled radius, Ξ, from Table 2, and keeping in mind that $H_0 = 50$ and 70 km s^{-1} Mpc^{-1} have been assumed in FM01 and KLA01 simulations, respectively. The result is:

$$7.12786\ 10^{-7} \leq (C_\delta)_{NFW,FM} \leq 5.70229\ 10^{-6} \quad ; \tag{40a}$$

$$5.93342\ 10^{-7} \leq (C_\delta)_{MOA,FM} \leq 4.74673\ 10^{-6} \quad ; \tag{40b}$$

$$1.05903\ 10^{-5} \leq (C_\delta)_{NFW,KLA} \leq 8.47224\ 10^{-5} \quad ; \tag{40c}$$

$$8.12553\ 10^{-6} \leq (C_\delta)_{MOA,KLA} \leq 6.50043\ 10^{-5} \quad ; \tag{40d}$$

mass	FM01				KLA01			
$\log \frac{M}{M_{10}}$	σ_0	b_1	b_2	$\log b_2$	σ_0	b_1	b_2	$\log b_2$
-1	15.08	1.00 10^1	3.43 10^2	2.535	4.200	1.72 10^1	7.41 10^0	0.870
0	11.85	2.75 10^1	1.66 10^3	3.221	3.300	4.73 10^1	3.59 10^1	1.555
1	8.61	8.14 10^1	6.38 10^3	3.805	2.400	1.40 10^2	1.38 10^2	2.141
2	5.71	2.64 10^2	1.86 10^4	4.270	1.590	4.55 10^2	4.02 10^2	2.604
3	3.66	8.89 10^2	4.90 10^4	4.690	1.020	1.53 10^3	1.06 10^3	3.026
4	2.05	3.42 10^3	8.61 10^4	4.935	0.570	5.90 10^3	1.85 10^3	3.268
5	0.937	1.61 10^4	8.23 10^4	4.915	0.261	2.77 10^4	1.77 10^3	3.249
6	0.345	9.43 10^4	4.11 10^4	4.613	0.096	1.62 10^5	8.84 10^2	2.947

Table 11: The mass (in decimal logarithm and unit $M_{10} = 10^{10} M_\odot$), the present-day rms mass excess, $\sigma_0 = < (\delta M/M)_0^2 >^{1/2}$, and the parameters, $b_1 = \bar{\nu}_{rec} \zeta_{max} R_{max}/\mathrm{kpc}$, $b_2 = \delta/(\bar{\nu}_{rec}^3 C_\delta \zeta_{max})$, related to top-hat, spherical perturbations with same mass spectrum as in Gunn (1987), but normalized to cosmological models assumed in FM01 and KLA01 simulations, respectively. The plot of the mass spectrum (Gunn 1987) has been assumed to reproduce only the growing mode.

in connection with both NFW and MOA density profiles, related to both FM01 and KLA01 simulations.

With regard to FM01 ($\sigma_8 = 0.7$) and KLA01 ($\sigma_8 = 0.9$) simulations, the mass enclosed within a spherical region of radius $R_8 = 8h^{-1}$ Mpc, is:

$$(M_8)_{FM} = 2.021868\ 10^5 M_{10} \quad ; \tag{41a}$$

$$(M_8)_{KLA} = 4.842291\ 10^4 M_{10} \quad ; \tag{41b}$$

for a formal derivation, see Appendix A. The normalization of top-hat, spherical perturbations with same spectrum as in Gunn (1987), to the above values, demands a multiplication of the rms mass excess plotted in Gunn (1987) by a factor of 14/13 and 3/10, respectively. The related values, together with some other parameters which are characteristic of top-hat, spherical perturbations, are listed in Table 11. The parameter, δ, expressed by Eqs. (39), is plotted as a function of the mass, for lower and upper values of the factor, C_δ, expressed by Eq. (40), and mean peak heights $\bar{\nu}_{rec} = 1, 2, 3, 4$, in Fig. 9, where the values deduced from FM01 (top panel) and KLA01 (bottom panel) simulations, in connection with MOA (top panel) and NFW (bottom panel)

density profiles, respectively, are also represented. In both cases it is apparent that, for increasing masses, simulated haloes correspond to fitting, top-hat haloes with increasing (mean) peak height.

The occurrence of cosmological constant changes the value of the treshold, beyond which density perturbations are expanding forever (e.g., Lokas & Hoffman 2001a,b). The mass of the critical density perturbation, related to an infinite turnaround radius, is marked by a vertical line in Fig. 9, from the left to the right for increasing peak height.

Keeping in mind that, for a fixed peak, upper curves are related to no acquisition of angular momentum ($\zeta_{vir} = 8$) and lower curves are related to maximal, allowed acquisition of angular momentum ($\zeta_{vir} = 1$), the correspondence between simulated and fitting, spherical, top-hat haloes implies an efficient acquisition of angular momentum, especially for low masses. On the other hand, with regard to FM01 runs, simulated haloes - especially at low masses - appear to be consistent with fitting, spherical, top-hat haloes with mean peak heights within the range $1 \lesssim \bar{\nu}_{rec} \lesssim 2$, contrary to what would be expected, $\bar{\nu}_{rec} \gtrsim 2$; with regard to KLA01 runs, the above mentioned discrepancy disappears.

5 Concluding remarks

Simulated dark matter haloes have been fitted by self-similar, universal density profiles, where the scaled parameters depend only on a scaled (truncation) radius, $\Xi = R/r_0$, which, in turn, has been supposed to be independent of the mass and the formation redshift. The further assumption of a lognormal distribution (for a selected mass bin) of the scaled radius, or concentration, in agreement with the data from a large statistical sample of simulated haloes (Bullock et al., 2001), has allowed (at least to a first extent) a normal or lognormal distribution for other scaled parameters, via the same procedure which leads to the propagation of the errors.

A criterion for the choice of the best fitting density profile has been proposed, with regard to a set of high-resolution simulations, where some averaging procedure on scaled density profiles has been performed, in connection with a number of fitting density profiles. To this aim, a minimum value of the ratio, $|x_{\overline{\eta}}|/\sigma_{s\,\overline{\eta}} = |\overline{\eta} - \eta^*|/\sigma_{s\,\overline{\eta}}$, has been required to yield the best fit, where $\overline{\eta}$ is the arithmetic mean over the whole set; η^* is its counterpart related to

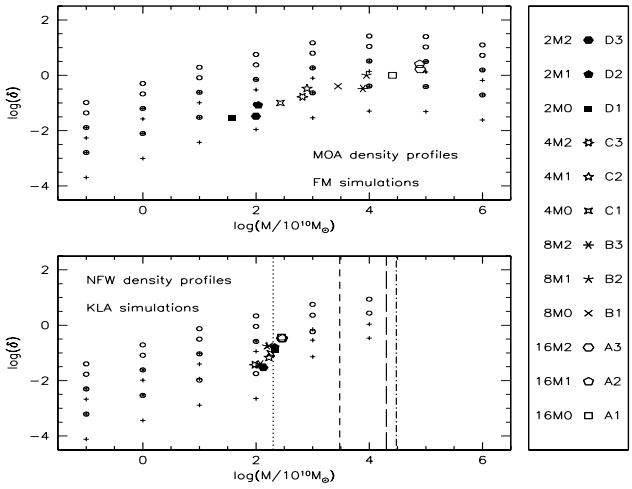

Figure 9: The dimensionless parameter, δ, vs. the fitting mass, M, for top-hat, spherical perturbations, with no (open circles) and maximum allowed (crosses) acquisition of angular momentum, according to Eqs. (40b) and (40c), in connection with MOA (top panel) and NFW (bottom panel) density profiles. For each mass and class of symbols, values from down to up are related to mean peak heights at recombination epoch, $\bar{\nu}_{rec} = 1, 2, 3, 4$, respectively. The mass of the critical density perturbation, for which the turnaround radius is infinite, is marked by a vertical line, from the left to the right for increasing peak height (bottom panel). Values related to FM01 (top panel) and KLA01 (bottom panel) simulations are also represented, with same symbol captions as in Figs.1-4 and 5-8, respectively. Passing from NFW to MOA density profile for each set of simulations, would lower values related to top-hat, spherical perturbations, by about one dex, and vice versa.

the fitting density profile; $\sigma_{s\overline{\eta}}$ is the standard deviation from the mean; and η is a selected, scaled i.e. dimensionless parameter.

The above criterion has been applied to a pair of sets each made of a dozen of high-resolution simulations, FM01 (Fukushige & Makino 2001) and KLA01 (Klypin et al. 2001), in connection with two currently used density profiles, NFW (e.g., Navarro et al. 1997) and MOA (e.g., Moore et al. 1999), where the dependence of the scaled radius on the mass and the formation redshift, may be neglected to a first extent. With regard to FM01 and KLA01 samples, the best fit has revealed to be MOA and NFW, respectively. In addition, the above results have been found to hold also in dealing with rms errors derived via the propagation of the errors, with regard to the distributions of scaled parameters. The sensitivity error of simulations has also been estimated and shown to be less than the related, standard deviation, that is a necessary condition for detectability of accidental errors.

Some features of the early evolution of dark matter haloes represented by fitting density profiles, have been discussed in the limit of the spherical top-hat model. Though the related matter distributions have appeared to be poorly representative of simulated haloes, unless the (mean) peak height is an increasing function of the mass, the results have been shown to be consistent, provided considerable acquisition of angular momentum took place during the expansion phase.

6 acknowledgements

We thank A. Gardini, L. Moscardini, E. Rasia, and G. Tormen for helpful discussions, and E. Lokas for enlightening explanations on Lokas & Hoffman papers referenced below. We are also grateful to S.H. Hansen for pointing our attention to a paper of his, referenced below, and related comments.

References

[1] Adams, F.C., Fatuzzo, M. 1996, ApJ 464, 256

[2] Bullock, J. S., Kolatt, T. S., Sigad, Y., Somerville, R. S., Kravtsov, A. V., Klypin, A. A., Primack, J. R., Dekel, A. 2001, MNRAS 321, 559

[3] Caimmi, R. 1980, ApSS 71, 415

[4] Caimmi, R., Secco, L., Andriani, E. 1990, ApSS 168, 131

[5] Caimmi, R., Marmo, C. 2003, NewA 8, 119

[6] Cole, S., Lacey, C. 1996, MNRAS 281, 716

[7] De Zeeuw T. 1985, MNRAS 216, 273

[8] Dubinski, J., Carlberg, R.G. 1991, ApJ 378, 496

[9] Fukushige, T., Makino, J. 2001, ApJ 557, 533 (FM01)

[10] Fukushige, T., Makino, J. 2003, ApJ 588, 674 (FM03)

[11] Fukushige, T., Kawai, A., Makino, J. 2004, ApJ 606, 625

[12] Ghigna, S., Moore, B., Governato, F., Lake, G., Quinn, T., Stadel, J. 2000, ApJ 544, 616

[13] Gunn, J.E. 1987, *The Galaxy*, NATO ASI Ser. C207, D. Reidel Publ. Co., Dordrecht, p. 413

[14] Hansen, S.H. 2004, MNRAS submitted (astro-ph/0405371)

[15] Hernquist, L. 1990, ApJ 356, 359

[16] Klypin, A., Kravtsov, A.V., Bullok, J.S., Primack, J.R. 2001, ApJ 554, 903 (KLA01)

[17] Lokas, E.L., 2002, preprint (astro-ph/0112031)

[18] Lokas, E.L., Hoffman, Y. 2001a, in Spooner N.J.C., Kudriavtsev V., eds., Proc. 3rd International Workshop, *The Identification of the Dark Matter*, World Scientific, Singapore, p.121 (astro-ph/0011295)

[19] Lokas, E.L., Hoffman, Y. 2001b, MNRAS submitted (astro-ph/0108283)

[20] Lokas, E.L., Hoffman, Y. 2002, in preparation

[21] Moore, B., Governato, F., Quinn, T., Stadel, J., Lake, G. 1998, ApJ 499, L5

[22] Moore, B., Quinn, T., Governato, F., Stadel, J., Lake, G. 1999, MNRAS 310, 1147 (MOA99)

[23] Moscardini, L. 1993, Rend. Sem. Mat. Univ. Pol. Torino 51, 249

[24] Mücket, J.P., Hoeft, M. 2003, A&A 404, 809

[25] Navarro, J.F., Frenk, C.S., White, S.D.M. 1995, MNRAS 275, 720

[26] Navarro, J.F., Frenk, C.S., White, S.D.M. 1996, ApJ 462, 563

[27] Navarro, J.F., Frenk, C.S., White, S.D.M. 1997, ApJ 490, 493 (NFW97)

[28] Oliva, P.R., Terrasi, F. 1976, *Elaborazione Statistica dei Risultati Sperimentali*, Liguori Editore, Napoli

[29] Padoan, P., Nordlund, A., Jones, B.J.R. 1997, MNRAS 288, 145

[30] Peebles, P.J.E. 1980, *The Large-Scale Structure of the Universe*, Princeton Univ. Press, New Jersey

[31] Peebles, P.J.E. 1993, *Principle of Physical Cosmology*, Princeton Univ. Press, New Jersey

[32] Syer, D., White, S. D. M. 1998, MNRAS 293, 337

[33] Taylor, J.R. 2000, *Introduzione all'analisi degli errori*, Zanichelli, Bologna

[34] Tasitsiomi, A., Kravtsov, A.V., Gottlöber, S., Klypin, A.A. 2004, ApJ 607, 125

[35] Tormen, G., Bouchet, F.R., White, S.D.M. 1997, MNRAS 286, 865

[36] Zeldovich, J.B., Novikov, I.D. 1982, *Struttura ed evoluzione dell'Universo*, Mir, Moscow

[37] Zhao, H.S. 1996, MNRAS 278, 488

7 Appendix

7.1 A. Some properties of spherical, top-hat density perturbations

With regard to a special class of QCDM cosmological models, where quintessence obeys the equation of state $p_\Psi = w\rho_\Psi$ relating its density, ρ_Ψ, to its pressure, p_Ψ, via a time-independent parameter or quintessence index, w, where $-1 \leq w < 0$, the following relations hold (e.g., Lokas 2002; Lokas & Hoffman 2002):

$$\frac{\mathrm{d}a}{\mathrm{d}t} = \frac{H_0}{\phi(a)} \quad ; \qquad a = \frac{R}{R_0} = \frac{1}{1+z} \quad ; \tag{42}$$

$$\phi(a) = \left[1 + \Omega_0 \left(a^{-1} - 1\right) + \Psi_0 \left(a^{-1-3w} - 1\right)\right]^{-1/2} \quad ; \tag{43}$$

$$\Omega(z) = \Omega_0 (1+z)^3 \frac{H_0^2}{H^2(z)} \quad ; \tag{44}$$

$$\Psi(z) = \Psi_0 (1+z)^{3(1+w)} \frac{H_0^2}{H^2(z)} \quad ; \tag{45}$$

$$\frac{H^2(z)}{H_0^2} = (1+z)^2(1+\Omega_0 z) + \Psi_0 (1+z)^{3(1+w)} \left[1 - (1+z)^{-(1+3w)}\right] \quad ; \tag{46}$$

where a is the scale factor normalized to unity at present, z is the redshift, Ω and Ψ the density parameter of matter and quintessence, respectively, H the Hubble parameter, and the index 0 denotes the current time. In the limit of a vanishing quintessence, Eqs. (42), (44), and (46) reduce to their counterparts in cosmological models with sole matter and radiation (e.g., Zeldovich & Novikov 1982, Chap. III, §4). The special case, $w = -1$, corresponds to the cosmological constant.

An equivalent expression of Eqs. (44) and (45), using (46), is:

$$\Omega^{-1}(z) = 1 + \frac{1}{1+z} \frac{1 - \Omega_0 - \Psi_0}{\Omega_0} + (1+z)^{3w} \frac{\Psi_0}{\Omega_0} \quad ; \tag{47}$$

$$\Psi^{-1}(z) = 1 + \frac{\Omega_0}{\Psi_0} (1+z)^{-3w} \left[1 + \frac{1}{1+z} \frac{1 - \Omega_0 - \Psi_0}{\Omega_0}\right] \quad ; \tag{48}$$

and Eq. (47) allows the validity of the inequality:

$$1+\frac{1}{1+z}\frac{1-\Omega_0-\Psi_0}{\Omega_0+\Psi_0}\leq\Omega^{-1}(z)\leq 1+\frac{1}{1+z}\frac{1-\Omega_0}{\Omega_0}\quad;\qquad -1\leq w\leq -\frac{1}{3}\quad; \tag{49}$$

which shows that the evolution of the matter density parameter in a cosmological model defined by assigned values of (Ω_0,Ψ_0), is comprised between its counterparts related to cosmological models defined by $(\Omega_0,0)$ and $(\Omega_0+\Psi_0,0)$, respectively.

With regard to the function, $\phi(a)$, defined by Eq. (43), a detailed analysis involving the solution of a third-degree equation yields the final result:

$$\left[1+\Omega_0\left(a^{-1}-1\right)\right]^{-1/2}\leq\phi(a)<\left[1+\frac{\Omega_0}{2}\left(a^{-1}-1\right)\right]^{-1/2}\quad;\qquad \Omega_0\geq 0.25\quad; \tag{50}$$

which shows that the evolution of the scale factor in a cosmological model defined by assigned values of (Ω_0,Ψ_0), is comprised between its counterparts related to cosmological models defined by $(\Omega_0/2,0)$ and $(\Omega_0,0)$, respectively, provided $\Omega_0\geq 0.25$.

With regard to the Hubble parameter, $H(t)$, defined by Eq. (46), a detailed analysis involving the solution of a transcendental equation yields the final result:

$$\frac{1}{2}(1+z)^2(1+\Omega_0 z)<\frac{H^2(z)}{H_0^2}\leq(1+z)^2(1+\Omega_0 z)\quad;\qquad \Omega_0\geq 0.25\quad; \tag{51}$$

which shows that the evolution of the Hubble parameter in a cosmological model defined by assigned values of (Ω_0,Ψ_0,H_0), is comprised between its counterparts related to cosmological models defined by $(\Omega_0,0,H_0)$ and $(\Omega_0,0,H_0/\sqrt{2})$, respectively, provided $\Omega_0\geq 0.25$.

Cosmological models with sole matter and radiation evolve at the same rate in the limit $|1-\Omega^{-1}|\ll 1$ i.e. at early times (e.g., Zeldovich & Novikov 1982, Chap. III, §4) and, owing to inequalities (49), (50), and (51), the same holds for cosmological models with quintessence. In the above mentioned limit, the matter density of the Hubble flow, ρ_h, reads (e.g., Peebles 1993, Chap. II, §13):

$$\rho_h=\frac{3}{8\pi}\frac{H_0^2\Omega_0}{G}(1+z)^3\quad; \tag{52}$$

where G is the constant of gravitation.

The combination of Eqs. (37) and (52) yields:

$$\bar{\rho}_{vir} = \frac{3}{8\pi}\zeta_{max}\zeta_{vir}\frac{H_0^2\Omega_0}{G}(1+z_{rec})^3\left[\left(\frac{\delta M^*}{M}\right)_{rec}\right]^3 \quad ;$$
$$|1-\Omega_{rec}^{-1}| \ll \left(\frac{\delta M^*}{M}\right)_{rec} \ll 1 \quad ; \tag{53}$$

in the framework of the top-hat, spherical model, related to a flat universe with vanishing quintessence, the growing mode of the density perturbation attains the present-day value (e.g., Peebles 1980, Chap. II, §15):

$$\left(\frac{\delta M}{M}\right)_0 = \frac{3}{5}\left(\frac{\delta M^*}{M}\right)_{rec}(1+z_{rec}) \quad ; \tag{54}$$

and the combination of Eqs. (53) and (54) yields Eq. (38).

In addition, the combination of Eqs. (34), (35), (52), and (54) produces:

$$\bar{\nu}_{rec}\zeta_{max}R_{max} = \frac{3}{5}\left(\frac{H_0^2\Omega_0}{2G}\right)^{-1/3} M^{1/3}\left\langle\left[\left(\frac{\delta M}{M}\right)_0\right]^2\right\rangle^{-1/2} \; ; \; |1-\Omega_{rec}^{-1}| \ll 1; \tag{55}$$

where the mass excess has been expressed as the product of the present-day rms mass excess and the peak height at recombination epoch, averaged over the whole volume, that is:

$$\left(\frac{\delta M}{M}\right)_{rec} = \bar{\nu}_{rec}\left\langle\left[\left(\frac{\delta M}{M}\right)_{rec}\right]^2\right\rangle^{1/2} \quad ; \tag{56}$$

for more details see e.g., Caimmi et al. (1990). Of course, Eq. (55) makes a lower limit to the product, $\bar{\nu}_{rec}R_{max}$, as Eq. (34) holds in the limit of a vanishing quintessence.

On the other hand, in open or flat universes, density perturbations below a treshold are destined to expand forever. In the special case of cosmological constant, the critical value is (e.g., Lokas & Hoffman 2001a,b):

$$\left[\left(\frac{\delta M}{M}\right)_{rec}\right]_\infty = \frac{U(\Lambda_{rec})}{\Omega_{rec}} - 1 \quad ; \tag{57a}$$
$$U(\Lambda) = 1 + \frac{5}{4}\Lambda + \frac{3}{4}\frac{\Lambda(8+\Lambda)}{T(\Lambda)} + \frac{3}{4}T(\Lambda) \quad ; \tag{57b}$$
$$T(\Lambda) = \Lambda^{1/3}\left[8 - \Lambda^2 + 20\Lambda + 8(1-\Lambda)^{3/2}\right]^{1/3} \quad ; \tag{57c}$$

where the turnaround occurs at an infinite radius.

With regard to FM01 and KLA01 simulations, the present-day rms mass excess in a spherical region of radius $R_8 = 8h^{-1}$ Mpc, takes the value:

$$(\sigma_8)_{FM} = \left\{ \left\langle \left[\left(\frac{\delta M}{M_8} \right)_0 \right]^2 \right\rangle^{1/2} \right\}_{FM} = 0.7 \quad ; \tag{58a}$$

$$(\sigma_8)_{KLA} = \left\{ \left\langle \left[\left(\frac{\delta M}{M_8} \right)_0 \right]^2 \right\rangle^{1/2} \right\}_{KLA} = 0.9 \quad ; \tag{58b}$$

owing to the general definition of mass excess:

$$\frac{\delta M}{M} = \frac{\bar{\rho} - \rho_h}{\rho_h} \quad ; \tag{59}$$

the mass within the region under consideration may be obtained using Eqs. (52), (58), and (59). The result is:

$$M_8 = 2^8 \ 10^9 \ (1 + \sigma_8) \frac{H_0^2 \Omega_0}{h^3 G} \quad ; \tag{60}$$

which may be specified for any flat cosmological model with assigned values of H_0, Ω_0, and σ_8.

7.2 B. Determination of fitting haloes to FM01 and KLA01 simulated haloes, with regard to NFW and MOA density profiles

Given a selected, FM01 simulated halo among the runs listed in Table 3 i.e. for which the values of the parameters, M_{200}, r_{200}, and δ, are known, we aim to derive the values of the scaling density, ρ_0, and the scaling radius, r_0, related to the corresponding, fitting halo, and then the remaining parameters, in connection with both NFW and MOA density profiles. The total mass of the simulated halo, M, appears in FM01 prescriptions, expressed by Eqs. (4) and (5), but the related values are not reported therein. Then the key parameter is the scaled radius, ξ_{200}.

Owing to the general definition of scaled radius, Eq. (5a) may be written under the equivalent form:

$$\xi_{200} = \frac{r_{200}}{r_0} = C_r^{-1} \delta^{1/3} \frac{r_{200}}{\mathrm{kpc}} \left(\frac{M}{\mathrm{M}_{10}} \right)^{-2/3} \quad ; \tag{61}$$

on the other hand, the particularization of the general expression of the mass enclosed within a generic, isopycnic surface, to the case under discussion, via Eqs. (2) and (3), reads:

$$M_{200} = 3 M_0 \int_0^{\xi_{200}} f(\xi) \xi^2 \, \mathrm{d}\xi \quad ; \tag{62}$$

and the combination of Eqs. (61) and (62) produces a transcendental equation in M, which can be solved in connection with an assigned (NFW or MOA) density profile, provided the values of the parameters, C_r, δ, r_{200}, and M_{200}, are specified using the data listed in Table 3.

The knowledge of the total mass of the simulated halo, assumed to coincide with the mass of the fitting halo, M, allows the calculation of the scaling density, ρ_0, and the scaling radius, r_0, via Eqs. (4) and (5), and then the radius along a fixed direction, $R = \Xi r_0$, the scaling mass, M_0, appearing in Eq. (6), and the dimensionless parameter, κ, expressed by Eq. (8).

With regard to NFW density profiles, the particularization of Eq. (62) to the case under discussion, yields:

$$M_{200} = 12 M_0 \left[\ln(1 + \xi_{200}) - \frac{\xi_{200}}{1 + \xi_{200}} \right] \quad ; \tag{63}$$

where, owing to Eqs. (6) and (19):

$$\frac{1}{12} \frac{M_{200}}{M_0} = \frac{125}{28\pi} \frac{M_{200}}{M} \quad ; \tag{64}$$

and the combination of Eqs. (63) and (64) yields:

$$\frac{M_{200}}{M} = \frac{28\pi}{125} \left[\frac{1}{1 + \xi_{200}} - \ln \frac{1}{1 + \xi_{200}} - 1 \right] \quad ; \tag{65}$$

finally, the combination of Eqs. (5b), (61), and (65) produces the ultimate transcendental equation in M.

With regard to MOA density profiles, the particularization of Eq. (62) to the case under discussion, yields:

$$M_{200} = 4M_0 \ln\left(1 + \xi_{200}^{3/2}\right) \quad ; \tag{66}$$

where, owing to Eqs. (6) and (17):

$$\frac{1}{4}\frac{M_{200}}{M_0} = \frac{375}{56\pi}\frac{M_{200}}{M} \quad ; \tag{67}$$

and the combination of Eqs. (66) and (67) yields:

$$\frac{M_{200}}{M} = \frac{56\pi}{375}\ln\left(1 + \xi_{200}^{3/2}\right) \quad ; \tag{68}$$

finally, the combination of Eqs. (5b), (61), and (68), produces the ultimate transcendental equation in M.

The above procedure, via Eqs. (10)-(16), also holds for a selected, KLA01 simulated halo among the runs listed in Table 4, for which the values of the parameters, M_{vir}, r_{vir}, and δ, are known.

With regard to both NFW and MOA density profiles, some parameters related to fitting haloes, in connection with simulated haloes from FM01 and KLA01, are listed in Tables 7 and 8, respectively.

7.3 C. Sensitivity errors of dark matter halo simulations

Bearing in mind the general results listed in Tab. 1, together with Eq. (8), the scaled parameters, M/M_0, R/r_0, $\bar{\rho}/\rho_0$, and κ, depend only on the fitting density profile. For a selected choice of exponents (α, β, γ), fitting haloes depend on two parameters, (r_0, ρ_0), or (M, δ), via Eqs. (4) and (5).

Given a computer run with N identical particles of mass m, the sensitivity error with respect to the mass is clearly expressed as $\Delta M = m$. It follows that:

$$\Delta\frac{M_{200}}{M_0} = \left(1 + \frac{M_{200}}{M_0}\right)\frac{M_{200}}{M_0}\frac{m}{M_{200}} \quad ; \quad \Delta M_0 = \Delta M_{200} = m \quad ; \tag{69}$$

the second parameter, δ, is proportional to the present-day mass excess of the growing mode predicted by the top-hat model, $(\delta M/M)_0$, as:

$$\delta = C_\delta \left[\left(\frac{\delta M}{M} \right)_0 \right]^3 \frac{M}{\mathrm{M}_{10}} \quad ; \tag{70a}$$

$$C_\delta = \frac{125}{54} \zeta_{vir} C_r^3 \Xi^3 \frac{H_0^2 \Omega_0}{G} \frac{\mathrm{kpc}^3}{\mathrm{M}_{10}} \quad ; \tag{70b}$$

where Ω_0 is the present-day, matter density parameter ($\Omega_0 + \Lambda_0 = 1$), and ζ_{vir} depends on the evolution of the density perturbation during the expansion phase, and lies within the range $1 \leq \zeta_{vir} \leq 8$. For a formal demonstration, see Appendix A.

The repetition of the above procedure yields:

$$\Delta\delta = \delta \frac{3M_{200} + 2(\delta M)_0}{M_{200}(\delta M)_0} m = \delta \left[2 + 3 C_\delta^{1/3} \delta^{-1/3} \left(\frac{M_{200}}{\mathrm{M}_{10}} \right)^{1/3} \right] \frac{m}{M_{200}} \quad ; \tag{71a}$$

$$\Delta(\delta M)_0 = \Delta M_{200} = m \quad ; \tag{71b}$$

and the sensitivity error with respect to ρ_0 and r_0, by use of Eqs. (4) and (6), is:

$$\Delta\rho_0 = 3\rho_0 \frac{M_{200} + (\delta M)_0}{M_{200}(\delta M)_0} m = 3\rho_0 \left[1 + C_\delta^{1/3} \delta^{-1/3} \left(\frac{M_{200}}{\mathrm{M}_{10}} \right)^{1/3} \right] \frac{m}{M_{200}} \quad ; \tag{72}$$

$$\Delta r_0 = \frac{1}{3} r_0 \left[4 + 3 C_\delta^{1/3} \delta^{-1/3} \left(\frac{M_{200}}{\mathrm{M}_{10}} \right)^{1/3} \right] \frac{m}{M_{200}} \quad ; \tag{73}$$

finally, the further assumption $\Delta r_{200} = \Delta r_0$ allows the following results:

$$\Delta \frac{r_{200}}{r_0} = \frac{1}{3} \left(1 + \frac{r_{200}}{r_0} \right) \left[4 + 3 C_\delta^{1/3} \delta^{-1/3} \left(\frac{M_{200}}{\mathrm{M}_{10}} \right)^{1/3} \right] \frac{m}{M_{200}} \quad ; \tag{74}$$

$$\begin{aligned} \Delta \frac{\bar{\rho}_{200}}{\rho_0} &= \Delta \left(\frac{M_{200}}{M_0} \frac{r_0^3}{r_{200}^3} \right) \\ &= \frac{\bar{\rho}_{200}}{\rho_0} \left[5 + \frac{M_{200}}{M_0} + 3 C_\delta^{1/3} \delta^{-1/3} \left(\frac{M_{200}}{\mathrm{M}_{10}} \right)^{1/3} \right] \left(1 + \frac{r_0}{r_{200}} \right) \frac{m}{M_{200}} \quad ; \end{aligned} \tag{75}$$

$$\Delta\kappa_{200} = \kappa_{200} \left(1 + \frac{r_0}{r_{200}} \right) \left[2 + \frac{3}{2} C_\delta^{1/3} \delta^{-1/3} \left(\frac{M_{200}}{\mathrm{M}_{10}} \right)^{1/3} \right] \frac{m}{M_{200}} \quad ; \tag{76}$$

where Eqs. (4) and (7) have been used.

The sensitivity error of FM01 computer runs in dark matter halo simulations, expressed by Eqs. (69), (74), (75) and (76), may be calculated and compared with their rms counterparts, to see if a necessary condition for the detectability of accidental errors is satisfied, namely:

$$\Delta\eta \leq \sigma_\eta \quad ; \tag{77}$$

where $\eta = M_{200}/M_0,\ r_{200}/r_0,\ \bar{\rho}_{200}/\rho_0,\ \kappa_{200}$. To this aim, an inspection of Tabs. 3, 5, and 7, shows that the following inequalities hold:

$$\frac{m}{M_{200}} < 10^{-6} \quad ; \quad \frac{M_{200}}{M_0} < 20 \quad ; \quad \frac{r_{200}}{r_0} < 20 \quad ; \quad \frac{r_0}{r_{200}} < \frac{1}{2} \quad ; \tag{78a}$$

$$\frac{\bar{\rho}_{200}}{\rho_0} < 1 \quad ; \quad \kappa_{200} < 2.8 \quad ; \quad C_\delta^{1/3}\delta^{-1/3}\left(\frac{M_{200}}{\mathrm{M}_{10}}\right)^{1/3} < 0.2 \quad ; \tag{78b}$$

where upper values of C_δ have been used, in connection with the range $1 \leq \zeta_{vir} \leq 8$, according to Eq. (39b). The combination of Eqs. (69), (74), (75), (76), and (78) yields:

$$\Delta\frac{M_{200}}{M_0} < 10^{-3} \quad ; \quad \Delta\frac{r_{200}}{r_0} < 10^{-4} \quad ; \quad \Delta\frac{\bar{\rho}_{200}}{\rho_0} < 10^{-4} \quad ; \quad \Delta\kappa_{200} < 10^{-5} \quad . \tag{79}$$

The sensitivity errors of KLA01 computer runs in dark matter halo simulations, are expressed in the same way, provided u_{200} is replaced by u_{vir} therein, where $u = M,\ r,\ \bar{\rho},\ \kappa$. An inspection of Tabs. 4, 6, 8, shows that the following inequalities hold:

$$\frac{m}{M_{vir}} < 6\ 10^{-4} \quad ; \quad \frac{M_{vir}}{M_0} < 30 \quad ; \quad \frac{r_{vir}}{r_0} < 20 \quad ; \quad \frac{r_0}{r_{vir}} < 0.2 \quad ; \tag{80}$$

$$\frac{\bar{\rho}_{vir}}{\rho_0} < 0.02 \quad ; \quad \kappa_{vir} < 20 \quad ; \quad C_\delta^{1/3}\delta^{-1/3}\left(\frac{M_{vir}}{\mathrm{M}_{10}}\right)^{1/3} < 1.2 \quad ; \tag{81}$$

where upper values of C_δ have been used, in connection with the range $1 \leq \zeta_{vir} \leq 8$, according to Eq. (39b). Following the same procedure used for FM01, yields the final result:

$$\Delta\frac{M_{vir}}{M_0} < 1 \quad ; \quad \Delta\frac{r_{vir}}{r_0} < 4\ 10^{-2} \quad ; \quad \Delta\frac{\bar{\rho}_{vir}}{\rho_0} < 5\ 10^{-4} \quad ; \quad \Delta\kappa_{vir} < 6\ 10^{-2} \quad ; \tag{82}$$

The comparison between the sensitivity errors, expressed by Eqs. (79) and (82), and their rms counterparts, deduced from Table 9, shows that a necessary condition for the detectability of accidental errors, expressed by Eq. (77), is satisfied for both FM01 and KLA01 simulations. To this aim, it is worth remembering that $\sigma_{\bar{\eta}} = \sigma_\eta/\sqrt{N}$, where $N = 12$ in the case under consideration, according to the theory of the errors.

7.4 D. rms errors of distributions depending on scaled parameters

Let dark matter haloes be fitted by universal density profiles, expressed by Eq. (2), and let the distribution depending on the scaled radius, Ξ (or concentration with regard to NFW density profiles), be lognormal. The scaled mass enclosed within the generic scaled distance, ξ, and the related scaled mean density, are:

$$\frac{M(\xi)}{M_0} = 3\int_0^\xi f(\xi)\xi^2\,\mathrm{d}\xi \quad ; \tag{83}$$

$$\frac{\bar{\rho}(\xi)}{\rho_0} = \frac{3}{\xi}\int_0^\xi f(\xi)\xi^2\,\mathrm{d}\xi \quad ; \tag{84}$$

and the generalization of the dimensionless parameter, k, defined by Eq. (8), to the generic scaled radius, ξ, reads:

$$k(\xi) = C_r^{3/2}\xi^{3/2} \quad ; \tag{85}$$

where the constant, C_r, is determined by averaging on the results of simulations (FM01), and for the cases of interest it is expressed by Eqs. (5b) and (10).

The first derivatives of the functions on the left-hand side of Eqs. (83), (84), and (85), are:

$$\frac{\mathrm{d}(M/M_0)}{\mathrm{d}\xi} = 3f(\xi)\xi^2 \quad ; \tag{86}$$

$$\frac{\mathrm{d}(\bar{\rho}/\rho_0)}{\mathrm{d}\xi} = \frac{3}{\xi}\left[f(\xi) - \frac{1}{\xi^3}\frac{M(\xi)}{M_0}\right] \quad ; \tag{87}$$

$$\frac{\mathrm{d}k}{\mathrm{d}\xi} = \frac{3}{2}\frac{k(\xi)}{\xi} \quad ; \tag{88}$$

and, in addition:

$$\frac{\mathrm{d}\log\xi}{\mathrm{d}\xi} = \frac{1}{\ln 10}\frac{1}{\xi} \quad ; \tag{89}$$

following the standard rules of derivation.

Let us suppose that (i) the scaled parameters, η, $\eta = M_{trn}/M_0$, Ξ_{trn}, $\bar{\rho}_{trn}/\rho_0$, and k_{trn}, $trn = 200,\ vir$, as functions of $\log\Xi_{trn}$, are expressible as Taylor series where the starting point coincides with the expected value of the lognormal distribution of the concentration, $\Xi = \exp_{10}(\log\Xi_{trn})^*$; (ii) the convergence radius of the series under discussion exceeds at least three times the rms error of the lognormal distribution, $\sigma_{\log\Xi_{trn}}$, or in other words the convergence occurs at least within the range, $\log\Xi \mp 3\sigma_{\log\Xi_{trn}}$; (iii) the series under discussion can safely be approximated by neglecting all the terms of higher order with respect to the first. It is worth remembering that the propagation of the errors, and the related formulae currently used in literature, are grounded on the above mentioned assumptions.

Let $\phi(\xi)$ be a generic, derivable function of an independent variable, ξ. The application of the theorem of the derivative of a function of a function, where the second function is $\log\xi$, yields:

$$\frac{\mathrm{d}\phi}{\mathrm{d}\log\xi} = \frac{\mathrm{d}\phi}{\mathrm{d}\xi}\frac{\mathrm{d}\xi}{\mathrm{d}\log\xi} = \ln 10\ \xi\frac{\mathrm{d}\phi}{\mathrm{d}\xi} \quad ; \tag{90}$$

and the particularization to the scaled parameters considered here, reads:

$$\frac{\mathrm{d}(M/M_0)}{\mathrm{d}\log\xi} = 3\ln 10\ f(\xi)\xi^3 \quad ; \tag{91}$$

$$\frac{\mathrm{d}(\bar{\rho}/\rho_0)}{\mathrm{d}\log\xi} = 3\ln 10\left[f(\xi) - \frac{1}{\xi^3}\frac{M(\xi)}{M_0}\right] \quad ; \tag{92}$$

$$\frac{\mathrm{d}k}{\mathrm{d}\log\xi} = \frac{3}{2}\ln 10\ k(\xi) \quad ; \tag{93}$$

owing to Eqs. (86), (87), and (88).

On the other hand, the validity of the above assumptions implies that the relations:

$$\eta(\log\Xi_{trn}) = \eta(\log\Xi) + \left(\frac{\mathrm{d}\eta}{\mathrm{d}\log\Xi_{trn}}\right)_{\log\Xi}(\log\Xi_{trn} - \log\Xi) \quad ; \tag{94a}$$

$$\eta = \frac{M}{M_0},\ \Xi,\ \frac{\bar{\rho}}{\rho_0},\ k \quad ; \qquad trn = 200, vir \quad ; \tag{94b}$$

hold to a good extent. The combination of Eqs. (89), (91), (92), (93), and (94), yields:

$$\frac{M(\log \Xi_{trn})}{M_0} = \frac{M}{M_0} + 3 \ln 10 f(\Xi) \Xi^3 (\log \Xi_{trn} - \log \Xi) \quad ; \tag{95}$$

$$\Xi_{trn}(\log \Xi_{trn}) = \Xi + \ln 10 \Xi (\log \Xi_{trn} - \log \Xi) \quad ; \tag{96}$$

$$\frac{\bar{\rho}(\log(\Xi_{trn})}{\rho_0} = \frac{\bar{\rho}}{\rho_0} + 3 \ln 10 \left[f(\Xi) - \frac{1}{\Xi^3} \frac{M}{M_0} \right] (\log \Xi_{trn} - \log \Xi) \quad ; \tag{97}$$

$$k(\log \Xi_{trn}) = k + \frac{3}{2} \ln 10 (\log \Xi_{trn} - \log \Xi) \quad ; \tag{98}$$

$$\tag{99}$$

where $M = M(\Xi)$, $\bar{\rho} = \bar{\rho}(\Xi)$, and $k = k(\Xi)$, for sake of brevity.

The scaled parameter, $\log \Xi_{trn}$, may be considered as a physical quantity to be measured directly. Accordingly, the distribution depending on $\log \Xi_{trn}$ has necessarily to be normal. A theorem related to the theory of errors ensures that the scaled parameters, η, defined by Eq. (94), also follow normal distributions, whose expected values and rms errors, via Eqs. (95), (96), (97), and (98), are expressed as:

$$\eta^* = \frac{M}{M_0}, \ \Xi, \ \frac{\bar{\rho}}{\rho_0}, \ k \quad ; \tag{100}$$

$$\sigma_\eta = \left| \left(\frac{\mathrm{d}\eta}{\mathrm{d} \log \Xi_{trn}} \right)_{\log \Xi} \right| \sigma_{\log \Xi} \quad ; \tag{101}$$

and the last relation, owing to Eqs. (89), (91), (92), and (93), takes the explicit form:

$$\sigma_{M/M_0} = 3 \ln 10 \ \Xi^3 f(\Xi) \ \sigma_{\log \Xi} \quad ; \tag{102}$$

$$\sigma_\Xi = \ln 10 \ \Xi \ \sigma_{\log \Xi} \quad ; \tag{103}$$

$$\sigma_{\bar{\rho}/\rho_0} = 3 \ln 10 \left| f(\Xi) - \frac{1}{\Xi^3} \frac{M}{M_0} \right| \sigma_{\log \Xi} \quad ; \tag{104}$$

$$\sigma_k = \frac{3}{2} \ln 10 \ k \ \sigma_{\log \Xi} \quad ; \tag{105}$$

for the scaled parameters under consideration.

Starting from Eq. (101), after replacing η with $\log \eta$, and using Eq. (89), after replacing ξ with η, yields an expression of the rms errors of lognormal

distributions, in terms of their counterparts related to normal distributions. The result is:

$$\sigma_{\log\eta} = \frac{1}{\ln 10}\frac{1}{\eta}\left|\left(\frac{\mathrm{d}\eta}{\mathrm{d}\log\Xi_{trn}}\right)_{\log\Xi}\right|\sigma_{\log\Xi} \quad ; \tag{106}$$

or, after comparison with Eq. (101):

$$\sigma_{\log\eta} = \frac{1}{\ln 10}\frac{1}{\eta}\,\sigma_{\eta} \quad ; \tag{107}$$

which, owing to Eqs. (102), (103), (104), and (105), take the explicit form:

$$\sigma_{\log(M/M_0)} = 3\Xi^3 f(\Xi)\left(\frac{M}{M_0}\right)^{-1}\sigma_{\log\Xi} \quad ; \tag{108}$$

$$\sigma_{\log\Xi} = \sigma_{\log\Xi} \quad ; \tag{109}$$

$$\sigma_{\log(\bar{\rho}/\rho_0)} = 3\left|f(\Xi) - \frac{1}{\Xi^3}\frac{M}{M_0}\right|\left(\frac{\bar{\rho}}{\rho_0}\right)^{-1}\sigma_{\log\Xi} \quad ; \tag{110}$$

$$\sigma_{\log k} = \frac{3}{2}\,\sigma_{\log\Xi} \quad ; \tag{111}$$

where the identity has been written for sake of completeness.

7.5 E. Random model: the concentration distribution as a result of the central limit theorem

Dark matter halo and star formation take place in a similar fashion, namely a transition from an undifferentiated fluid to substructures. Though a molecular cloud is neither expanding nor subjected to the Copernican principle, contrary to the Hubble flow, still the above mentioned processes are expected to exhibit some common features.

The initial mass function in a star generation may safely be fitted by a lognormal distribution (e.g., Adams & Fatuzzo 1996; Padoan et al. 1997), which, in turn, can be interpreted in terms of the central limit theorem (Adams & Fatuzzo 1996). On the other hand, data from a statistical sample of about five thousands of simulated dark matter haloes (Bullock et al. 2001), show - to a good extent - a lognormal distribution of the concentration within mass bins of (0.5-1.0)$\times 10^n h^{-1}\mathrm{M}_\odot$, where $11 \leq n \leq 14$ and n is an integer.

Here we adopt a statistical approach to the calculation of the lognormal distribution of the concentration, following the same procedure used by Adams & Fatuzzo (1996), in dealing with the initial mass function of a star generation. To this aim, first let us suppose that a transformation exists between initial conditions and the final properties of the dark matter halo with assigned mass.

Given a cosmological model and a perturbation spectrum, the initial conditions of a simulation are defined by a generation of complex numbers with a phase randomly distributed in the range $0 \leq \phi < 2\pi$ and with amplitude normally distributed, where the variance is provided by the selected spectrum, in the simplest case of a Gaussian distributed random field. For further details see e.g., Moscardini (1993); Tormen et al. (1997).

Given a universal density profile, assumed to fit to dark matter haloes under consideration, the final properties are related to the scaled radius, or the concentration with regard to NFW density profiles, via the results listed in Table 1.

Second, let us suppose that the transformation under consideration is expressible as a product:

$$\Xi_{trn} = A \prod_{j=1}^{n} \beta_j^{\gamma_j} = \prod_{j=1}^{n} \alpha_j \quad ; \tag{112}$$

where the constant, A, and the exponents, γ_j, are fixed, and the variables, β_j or α_j, are conceived as random variables. Though Eq. (112) cannot be motivated by the existence of a semiempirical relation, as in the case of star formation (Adams & Fatuzzo 1996), neverthless it cannot be excluded unless further knowledge about the genesis of dark matter haloes will be available.

The central limit theorem holds provided the random variables, α_j, appearing in Eq. (112), are completely independent, and their number, n, tends to infinite. For the more realistic case of a finite number of not completely independent random variables, the resulting distribution is expected to be different from a (log)normal distribution.

Taking the decimal logarithm on both sides of Eq. (112) yields:

$$\log \Xi_{trn} = \sum_{j=1}^{n} \log \alpha_j \quad ; \tag{113}$$

and the expected value of the distribution, $f_j(\log \alpha_j)\, \mathrm{d} \log \alpha_j$, depending on

the random variable, $\log \alpha_j$, is:

$$(\log \alpha_j)^* = \int_{-\infty}^{+\infty} \log \alpha_j f_j(\log \alpha_j) \, \mathrm{d} \log \alpha_j \quad ; \quad 1 \leq j \leq n \quad ; \tag{114}$$

accordingly, the error, $x_{\log \alpha_j}$, is:

$$x_{\log \alpha_j} = \log \alpha_j - (\log \alpha_j)^* = \log \frac{\alpha_j}{\alpha_j^*} \quad ; \tag{115a}$$

$$\alpha_j^* = \exp_{10}(\log \alpha_j)^* \quad ; \qquad 1 \leq j \leq n \quad ; \tag{115b}$$

where, of course, α_j^* is different from the expected value of the distribution, $f_j(\alpha_j) \, \mathrm{d}\alpha_j$, depending on the random variable, α_j.

The variance of the distribution, $f_j(x_{\log \alpha_j}) \, \mathrm{d}x_{\log \alpha_j}$, is:

$$\sigma^2_{\log \alpha_j} = \int_{-\infty}^{+\infty} x^2_{\log \alpha_j} f_j(x_{\log \alpha_j}) \, \mathrm{d}x_{\log \alpha_j} \quad ; \qquad 1 \leq j \leq n \quad ; \tag{116}$$

and the related, expected value, equals zero.

Let us define the random variable:

$$\zeta = \sum_{j=1}^{n} x_{\log \alpha_j} = \sum_{j=1}^{n} \log \frac{\alpha_j}{\alpha_j^*} = \sum_{j=1}^{n} \log \alpha_j - \sum_{j=1}^{n} \log \alpha_j^* \quad ; \tag{117}$$

and combine Eqs. (113) and (117), to obtain:

$$\log \Xi_{trn} = \zeta + \sum_{j=1}^{n} \log \alpha_j^* \quad ; \tag{118}$$

which is equivalent to:

$$\Xi_{trn} = \Xi^* \exp_{10}(\zeta) \quad ; \tag{119a}$$

$$\Xi^* = \prod_{j=1}^{n} \alpha_j^* \quad ; \tag{119b}$$

where, of course, Ξ^* is different from the expected value of the distribution, $f(\Xi_{trn}) \, \mathrm{d}\Xi_{trn}$, depending on the random variable, Ξ_{trn}.

The application of the central limit theorem to the distribution, $f(\zeta) \, \mathrm{d}\zeta$, depending on the random variable, ζ, yields (e.g., Adams & Fatuzzo 1996):

$$\sigma^2_{\zeta} = \sum_{j=1}^{n} \sigma^2_{\log \alpha_j} \quad ; \tag{120}$$

and aiming to find a distribution, $f(\tilde{\zeta})\,\mathrm{d}\tilde{\zeta}$, characterized by unit variance, $\sigma^2_{\tilde{\zeta}} = 1$, and null expected value, $\tilde{\zeta}^* = 0$, let us define the random variable:

$$\tilde{\zeta} = \frac{\zeta}{\sigma^2_{\zeta}} \quad ; \tag{121}$$

where, owing to the central limit theorem, the distribution is normal:

$$f(\tilde{\zeta})\,\mathrm{d}\tilde{\zeta} = \frac{1}{\sqrt{2\pi}} \exp\left(-\frac{\tilde{\zeta}^2}{2}\right)\,\mathrm{d}\tilde{\zeta} \quad ; \tag{122}$$

independent of the initial distributions, $f_j(x_{\log \alpha_j})\,\mathrm{d}x_{\log \alpha_j}$.

Taking the decimal logarithm of both sides of Eq. (119a), and using Eq. (121), yields:

$$\log \Xi_{trn} = \log \Xi^* + \zeta = \log \Xi^* + \sigma^2_{\zeta}\tilde{\zeta} \quad ; \tag{123}$$

and the distribution, $f(\Xi_{trn})\,\mathrm{d}\Xi_{trn}$, depending on the random variable, Ξ_{trn}, is lognormal. The related expected value and variance are:

$$(\log \Xi_{trn})^* = \log \Xi^* \quad ; \tag{124}$$

$$\sigma^2_{\log \Xi_{trn}} = \sigma^2_{\zeta} \quad ; \tag{125}$$

accordingly, the distribution reads:

$$f(\log \Xi_{trn})\,\mathrm{d}\log \Xi_{trn} = \frac{1}{\sqrt{2\pi}\sigma_{\zeta}} \exp\left[-\frac{(\log \Xi_{trn} - \log \Xi^*)^2}{2\sigma^2_{\zeta}}\right]\,\mathrm{d}\log \Xi_{trn} \tag{126}$$

and the decimal logarithm of the probability density, $f(\log \Xi_{trn})$, may be written as:

$$\log[f(\log \Xi_{trn})] = -\frac{1}{2}\log(2\pi) - \log \sigma_{\zeta} - \frac{1}{\ln 10}\frac{1}{2\sigma^2_{\zeta}}\left(\log \frac{\Xi_{trn}}{\Xi^*}\right)^2 \quad ; \tag{127}$$

where the first term on the right-hand side member may be conceived as a normalization constant.

The values of the expected value and the variance, expressed by Eqs. (124) and (125), related to the lognormal distribution, defined by Eq. (126), may be deduced from the results of simulations (e.g., Bullock et al. 2001). For further details on the procedure outlined above, see Adams & Fatuzzo (1996).

By analogy with the theory of measure, a computer run may be considered as an execution of measure operations, the related computer code as a measure instrument, the dark halo as a measure subject, and the sequences of random numbers used in the definition of initial conditions as contributors to the accidental error. Then the computer output may be thought about as a measure of the corresponding scaled parameter, which may be conceived as fluctuating around its fitting counterpart.

In addition, it is worth of note that the application of a least-squares or least-distances method in fitting simulated with universal density profiles (e.g., Dubinski & Carlberg 1991; KLA01; FM03) implies a (fiducial) normal distribution of the simulated density (in decimal logarithm) around the expected value deduced from the fitting density profile, at any fixed distance (in decimal logarithm). It is the particularization, to the case of interest, of a well known result of the theory of errors (e.g., Taylor 2000, Chap. 8, § 8.2).